Title :

Multivariate Analysis of Noise in Genetic Regulatory Networks

Authors :

Ryota Tomioka[a,b][1], Hidenori Kimura[b,c], Tetsuya J. Kobayashi[b], and Kazuyuki Aihara[b,d,e]

[a] Department of Mathematical Engineering and Information Physics, School of Engineering, The University of Tokyo, 7-3-1 Hongo, Bunkyo-ku, Tokyo 113-8656, Japan.

[b] Department of Complexity Science and Engineering, Graduate School of Frontier Sciences, The University of Tokyo, 7-3-1 Hongo, Bunkyo-ku, Tokyo 113-8656, Japan.

[c] Bio-Mimetic Control Research Center, The Institute of Physical and Chemical Research, 2271-130 Anagahora, Shimoshidami, Moriyama-ku Nagoya, 463-0003 Japan.

[d] Institute of Industrial Science, The University of Tokyo, 4-6-1 Komaba, Meguro-ku, Tokyo 153-8505, Japan.

[e] ERATO Aihara Complexity Modelling Project, JST, 45-18 Oyama, Shibuya-ku, Tokyo 151-0065, Japan.

Corresponding Author :

Ryota Tomioka

Aihara Laboratory,
Institute of Industrial Science,
The University of Tokyo,
4-6-1 Komaba, Meguro-ku, Tokyo 153-8505, Japan.

Email: ryotat@sat.t.u-tokyo.ac.jp
TEL: +81-3-5452-6693
FAX: +81-3-5452-6694

[1] Present address.

Abstract

Stochasticity is an intrinsic property of genetic regulatory networks due to the low copy numbers of the major molecular species, such as, DNA, mRNA, and regulatory proteins. Therefore, investigation of the mechanisms that reduce the stochastic noise is essential in understanding the reproducible behaviors of real organisms and is also a key to design synthetic genetic regulatory networks that can reliably work. We use an analytical and systematic method, the linear noise approximation of the chemical master equation along with the decoupling of a stoichiometric matrix. In the analysis of fluctuations of multiple molecular species, the covariance is an important measure of noise. However, usually the representation of a covariance matrix in the natural coordinate system, i.e., the copy numbers of the molecular species, is intractably complicated because reactions change copy numbers of more than one molecular species simultaneously. Decoupling of a stoichiometric matrix, which is a transformation of variables, significantly simplifies the representation of a covariance matrix and elucidates the mechanisms behind the observed fluctuations in the copy numbers. We apply our method to three types of fundamental genetic regulatory networks, that is, a single-gene autoregulatory network, a two-gene autoregulatory network, and a mutually repressive network. We have found that there are multiple noise components differently originating. Each noise component produces fluctuation in the characteristic direction. The resulting fluctuations in the copy numbers of the molecular species are the sum of these fluctuations. In the examples, the limitation of the negative feedback in noise reduction and the trade-off of fluctuations in multiple molecular species are clearly explained. The analytical representations show the full parameter dependence. Additionally, the validity of our method is tested by stochastic simulations.

Key words: stochastic gene expression, genetic regulatory network, noise reduction, linear noise approximation, decoupling of a stoichiometric matrix

1 Introduction

Control of intracellular noise is crucial for living organisms. Biochemical reactions are intrinsically noisy (Ozbudak *et al.*, 2002; Elowitz *et al.*, 2002; Blake *et al.*, 2003) due to the low copy numbers of the molecular species, such as DNA, mRNA, and regulatory proteins. However, most of the cellular events are ordered and reproducible despite the underlying randomness in their building blocks (Rao *et al.*, 2002). One important unsolved problem is the explanation of how robustness to this randomness in real organisms is achieved. Understanding such mechanisms not only gives deep insight into the design principles of real organisms, but also is a crucial key for engineering reliable synthetic genetic regulatory networks for biotechnological and therapeutic applications.

One strategy that can be used to reduce the noise is to increase the copy numbers of the molecular species enough so that the fluctuations become insignificant compared to the whole number of the molecular species. However, such strategies are energetically inefficient. The strategies that real organisms have developed seem to be both efficient and robust. A recent study of the embryo-to-embryo variability of morphogen protein profiles in *Drosophila* (Houchmandzadeh *et al.*, 2002) have revealed that, the Hb boundary position is precisely regulated at the downstream of the Bicoid gradient, which has high embryo-to-embryo variablity. Interestingly, the Hb protein profile displays high variability except at the center of embryo length, which is the exact position of the boundary. This result suggests that (i) in real organisms, not all fluctuations are fatal, (ii) organisms can reduce the fluctuations in significant molecular species at the cost of increasing fluctuations in the other molecular species that are less significant, and conversely (iii) when designing a synthetic genetic regulatory network, one might increase fluctuations in some of the molecular species just to reduce the fluctuations in the others. Thus, it is necessary to analyze the fluctuations of multiple molecular species. However, it is insufficient to analyze the fluctuation of each molecular species independently, because usually chemical reactions require two or more molecular species, thus the correlation between the fluctuations cannot be ignored. Therefore, we need to evaluate not only variance, but also covariance as statistical measures of noise in genetic networks.

Various methods for evaluating noise in genetic regulatory networks have been proposed recently. They are roughly categorized into two groups. Monte-Carlo simulations

of the chemical master equation (CME) based on the Gillespie method (Gillespie, 1977) are one of the most frequently used numerical methods (Arkin *et al.*, 1998; Elowitz & Leibler, 2000; Blake *et al.*, 2003). They can fully reproduce the probabilistic and discrete nature of biochemical reactions. However, they require huge computational time in order to obtain a reliable estimation of the distribution, especially in multivariate problems, and give us little intuition into those mechanisms behind specific observations which determine phenotypic noisy behaviors.

On the other hand, analytical methods using the probability generating functions (Berg, 1978; Peccoud & Ycart, 1995; Thattai & van Oudenaarden, 2001; Swain *et al.*, 2002), the Langevin equation (Ozbudak *et al.*, 2002; Simpson *et al.*, 2003), or the Fokker-Planck equation (Hasty *et al.*, 2000; Kepler & Elston, 2001) have also been applied to genetic regulatory networks. Although they clearly show the fundamental mechanisms that determine noise, they may become intractably difficult for nonlinear or multivariate problems.

In this paper, we apply an analytical and multivariate method called the *linear noise approximation* (LNA) (van Kampen, 1992) of the chemical master equation (CME), to evaluate the fluctuations around deterministic stable equilibrium states. It is rigorously derived from the CME and can be systematically applied to arbitrary N-dimensional problems.

In addition, we propose the decoupling of a stoichiometric matrix in advance to the LNA to facilitate analytical studies. When a given stoichiometric matrix is *decouplable*, there exist a transformation of variables, which (i) guarantees that each of the reaction channels changes only one variable for a single firing, (ii) diagonalizes the diffusion matrix, and (iii) simplifies the representation of the covariance matrix into a linear combination of N terms. These terms represent noise components that originate from different noise sources. Moreover, these noise components have characteristic magnitudes and directions (the definitions of the decomposition of noise and the decoupling of a stoichiometric matrix are given in Appendices A and B). Decoupling of a stoichiometric matrix enables us to understand the mechanisms behind mere observations, such as, how noise can be decomposed into its origins, in which direction the major noise component is, fluctuations in which molecular species can be reduced without affecting others, and which fluctuations cannot be.

We apply this method to investigate the multivariate stochasticity in three fundamental genetic regularity networks. That is, a single-gene autoregulatory network, a two-gene autoregulatory network, and a mutually repressive network. First, we consider a single-gene autoregulatory network in which dimers formed in solution bind to the DNA to repress the transcription. We show that autoregulations can reduce one of the two noise components, namely, the *protein birth and death noise*, but not the other noise component, namely, the *monomer-dimer fluctuation noise*. This is clearly shown in analytical representation of the covariance matrix. Additionally, we show that these two noise components produce fluctuations in the characteristic directions. Second, in order to investigate the mechanisms that can change direction of noise, we consider a two-gene autoregulatory network. We show that the direction of noise can be drastically changed by changing the balance between the positive regulation and the negative regulation. Furthermore, we demonstrate this by a biologically plausible network. Finally, we apply our method to a mutually repressive network to demonstrate that our method is applicable to systems with multiple equilibrium states.

This paper is organized as follows. In section 2, we model the stochastic dynamics of a genetic regulatory network with the CME and show the derivation of the LNA (van Kampen, 1992). In section 3, we show the main results of applying this method to three types of networks. In section 4, we discuss the advantages of our method, the connection with the previous studies, and the biological implications of our results. Additionally, Appendix A shows the definition of the decomposition of noise and the exact form of the decomposed 2×2 covariance matrix; Appendix B shows the definition of the decoupling of a stoichiometric matrix and the necessary and sufficient condition for a given stoichiometric matrix to be decouplable; Appendix C shows the proof of stability and uniqueness conditions; the parameter values used in this paper are listed in Appendix D; the comparison of the analytical results and stochastic simulations are shown in Appendix E.

2 Theory

2.1 Linear Noise Approximation

A genetic regulatory network can be modeled as a chemically reacting system consisting of N molecular species $\{\mathrm{S}_1, \ldots, \mathrm{S}_N\}$ and M reaction channels $\{\mathrm{R}_1, \ldots, \mathrm{R}_M\}$ inside a region

with a fixed volume Ω and at a constant temperature. We specify the dynamical state of the system by the copy numbers of molecular species $\boldsymbol{X} = (X_1, X_2, \ldots, X_N)^{\mathrm{T}} \in \mathbb{Z}^{+N}$, where $^{\mathrm{T}}$ denotes transposition. The *stoichiometric matrix* is defined as $A = \{a_{ij}\} \in \mathbb{Z}^{N\times M}$ where a_{ij} is the change in the copy number of S_i produced by a single firing of the reaction channel R_j. The *propensity function* $\boldsymbol{W}(\boldsymbol{X}) = (W_1(\boldsymbol{X}), \ldots, W_M(\boldsymbol{X}))^{\mathrm{T}}$ is defined as follows (Gillespie, 2000): $W_j(\boldsymbol{X})\Delta t$ denotes the probability that the reaction channel R_j fires within the next infinitesimal time interval Δt, given that the system is in a state $\boldsymbol{X}$, for $j = 1, \ldots, M$.

When there are sufficiently large copy numbers of molecular species, a propensity function can be rewritten as $\boldsymbol{W}(\boldsymbol{X}) \simeq \Omega \boldsymbol{w}(\boldsymbol{X}/\Omega)$ where $\boldsymbol{w}(\boldsymbol{x})$ is a function of the concentration $\boldsymbol{x} \equiv \boldsymbol{X}/\Omega$. Therefore, in the thermodynamic limit $\Omega \to \infty$, we obtain the well known macroscopic reaction rate equation (RRE) by taking the concentration $\boldsymbol{x}$ as the state variable and omitting the $\Omega^{-1/2}$ order fluctuation in $\boldsymbol{x}$, as follows:

$$\frac{\mathrm{d}\boldsymbol{x}}{\mathrm{d}t} = A\boldsymbol{w}(\boldsymbol{x}). \tag{1}$$

In mesoscopic systems with large but finite copy numbers, such as, genetic regulatory networks, $\boldsymbol{X}$ should be regarded as random variable $\boldsymbol{\mathcal{X}}$. The chemical master equation (CME) (van Kampen, 1992) is widely used to describe the time evolution of the probability density function (PDF) $P(\boldsymbol{X}; t) \equiv \mathrm{Prob}(\boldsymbol{\mathcal{X}}(t) = \boldsymbol{X})$, i.e., the probability that the system is in a state $\boldsymbol{X}$ at time t, under a certain initial distribution $P(\boldsymbol{X}; 0)$.

$$\frac{\mathrm{d}P(\boldsymbol{X}; t)}{\mathrm{d}t} = \sum_{j=1}^{M} \Big[W_j(\boldsymbol{X} - \boldsymbol{a}_j) P(\boldsymbol{X} - \boldsymbol{a}_j; t) - W_j(\boldsymbol{X}) P(\boldsymbol{X}; t) \Big], \tag{2}$$

where $\boldsymbol{a}_j = (a_{1j}, \ldots, a_{Nj})^{\mathrm{T}}$ is the stoichiometric coefficient of the reaction channel R_j.

We do not aim to solve the CME directly. Rather, we characterize the solution by the moments of $\boldsymbol{\mathcal{X}}$. We can obtain the following equation representing the time evolution of the first-order moment $\langle \boldsymbol{\mathcal{X}} \rangle$ by multiplying both sides of Eq. (2) by $\boldsymbol{X}$ and taking summation over all variables $X_1, \ldots, X_N$ (van Kampen, 1992):

$$\frac{\mathrm{d}\langle \boldsymbol{\mathcal{X}} \rangle}{\mathrm{d}t} = \langle A\boldsymbol{W}(\boldsymbol{\mathcal{X}}) \rangle \equiv \langle \boldsymbol{F}(\boldsymbol{\mathcal{X}}) \rangle . \tag{3}$$

Similarly, we can obtain the equation for the second-order moment $\left\langle \boldsymbol{\mathcal{X}} \boldsymbol{\mathcal{X}}^{\mathrm{T}} \right\rangle$ by multi-

plying both sides of Eq. (2) by $\boldsymbol{X}\boldsymbol{X}^{\mathrm{T}}$ and taking the summation (van Kampen, 1992):

$$\frac{\mathrm{d}\left\langle \boldsymbol{\mathcal{X}}\boldsymbol{\mathcal{X}}^{\mathrm{T}}\right\rangle}{\mathrm{d}t} = \left\langle \boldsymbol{F}(\boldsymbol{\mathcal{X}})\boldsymbol{\mathcal{X}}^{\mathrm{T}}\right\rangle + \left\langle \boldsymbol{\mathcal{X}}\boldsymbol{F}^{\mathrm{T}}(\boldsymbol{\mathcal{X}})\right\rangle + \left\langle D(\boldsymbol{\mathcal{X}})\right\rangle, \tag{4}$$

where the diffusion matrix (van Kampen, 1992) $D(\boldsymbol{X})$ is defined as follows:

$$D(\boldsymbol{X}) \equiv \left\{ d_{ij}(\boldsymbol{X}) \right\}_{ij}, \qquad d_{ij}(\boldsymbol{X}) \equiv \sum_{k=1}^{M} a_{ik}a_{jk}W_k(\boldsymbol{X}) \qquad (i,j=1,\ldots,N). \tag{5}$$

In general, the time evolutions of the moments are described by linear but infinite dimensional ODEs. The time evolution of the m-th order moment depends on the $d+m-1$-th order moment, where d denotes the dimension of the highest term of $\boldsymbol{X}$ in $\boldsymbol{W}(\boldsymbol{X})$. Accordingly, when $d \geq 2$, the time evolutions of any moments depend on higher moments that depend in turn on much higher moments and so on. Equations (3) and (4) become closed simultaneous ODE only when $\boldsymbol{W}(\boldsymbol{X})$ is a linear function of $\boldsymbol{X}$.

Now, we consider the case when the PDF $P(\boldsymbol{X};t)$ is distributed around the deterministic solution $\boldsymbol{X} = \Omega\boldsymbol{\phi}(t)$ tightly enough so that we can approximate $\boldsymbol{W}(\boldsymbol{X})$ by linearizing it around $\boldsymbol{X} = \Omega\boldsymbol{\phi}(t)$, where $\boldsymbol{\phi}(t)$ is the solution of the following deterministic equation, which is equivalent to the macroscopic RRE (1) in the thermodynamic limit $\Omega \to \infty$:

$$\frac{\mathrm{d}\Omega\boldsymbol{\phi}(t)}{\mathrm{d}t} = \boldsymbol{F}(\Omega\boldsymbol{\phi}(t)). \tag{6}$$

The state vector $\boldsymbol{\mathcal{X}}$ is decomposed as $\boldsymbol{\mathcal{X}} = \Omega\boldsymbol{\phi}(t) + \boldsymbol{\mathcal{E}}$, using the random variable $\boldsymbol{\mathcal{E}}$ to denote the deviation from the deterministic term $\Omega\boldsymbol{\phi}(t)$. Therefore, Eq. (3) can be rewritten as follows:

$$\frac{\mathrm{d}\left\langle \Omega\boldsymbol{\phi}(t) + \boldsymbol{\mathcal{E}}\right\rangle}{\mathrm{d}t} = \left\langle \boldsymbol{F}(\Omega\boldsymbol{\phi}(t)) + K(\boldsymbol{\phi}(t))\boldsymbol{\mathcal{E}} + O\left(|\boldsymbol{\mathcal{E}}|^2\right)\right\rangle, \tag{7}$$

where $K(\boldsymbol{\phi})$ is the Jacobian matrix of the deterministic system (Eq. (6)):

$$K(\boldsymbol{\phi}) \equiv \left.\frac{\partial F(\Omega\boldsymbol{x})}{\partial \Omega\boldsymbol{x}}\right|_{\boldsymbol{x}=\boldsymbol{\phi}} \left(\simeq \left.\frac{\partial A\boldsymbol{w}(\boldsymbol{x})}{\partial \boldsymbol{x}}\right|_{\boldsymbol{x}=\boldsymbol{\phi}} (\Omega \to \infty) \right).$$

Similarly rewriting Eq. (4) and truncating the $O(|\boldsymbol{\mathcal{E}}|^2)$ terms in the Taylor series of the both equations yield the following equations representing the time evolutions of $\boldsymbol{\mu} \equiv \langle \boldsymbol{\mathcal{E}} \rangle$

and $\Sigma \equiv \left\langle \boldsymbol{\mathcal{E}} \boldsymbol{\mathcal{E}}^{\mathrm{T}} \right\rangle - \left\langle \boldsymbol{\mathcal{E}} \right\rangle \left\langle \boldsymbol{\mathcal{E}} \right\rangle^{\mathrm{T}}$.

$$\frac{\mathrm{d}\boldsymbol{\mu}}{\mathrm{d}t} = K(\boldsymbol{\phi}(t))\boldsymbol{\mu}, \tag{8}$$

$$\frac{\mathrm{d}\Sigma}{\mathrm{d}t} = K(\boldsymbol{\phi}(t))\Sigma + \Sigma K^{\mathrm{T}}(\boldsymbol{\phi}(t)) + D(\Omega\boldsymbol{\phi}(t)) + \left.\frac{\partial D(\Omega\boldsymbol{x})}{\partial \Omega \boldsymbol{x}}\right|_{\boldsymbol{x}=\boldsymbol{\phi}(t)} \boldsymbol{\mu}. \tag{9}$$

Now, we have the closed simultaneous equations representing the time evolution of the mean $\boldsymbol{\mu}$ and the covariance matrix Σ of the random fluctuations around the deterministic solution.

Here, we make the following two assumptions:

1. Along the deterministic solution $\boldsymbol{\phi}(t)$, $K(\boldsymbol{\phi}(t))$ is stable, in other words, the real parts of all the eigenvalues of $K(\boldsymbol{\phi}(t))$ are negative for all $t \geq 0$.

2. The solution of Eq. (6) under a certain initial condition $\boldsymbol{\phi}(0) = \boldsymbol{\phi}_0$ is attracted to a stable equilibrium point $\boldsymbol{\phi}^{eq}$.

The first assumption is necessary to justify the linearization we have performed above. The second assumption is necessary to evaluate the fluctuations at deterministic stable equilibrium points as we show next.

It is well known that Eqs. (8) and (9) have a unique stable equilibrium point under the two assumptions shown above. Therefore, it is straightforward to show that there exists a stable distribution around $\boldsymbol{\phi}^{eq}$ with mean $\boldsymbol{\mu} = 0$ and covariance matrix Σ that satisfies the following equation called the Lyapunov equation:

$$K(\boldsymbol{\phi}^{eq})\Sigma + \Sigma K^{\mathrm{T}}(\boldsymbol{\phi}^{eq}) + D(\Omega\boldsymbol{\phi}^{eq}) = 0. \tag{10}$$

This equation can be solved for arbitrary N, because it can always be transformed into linear $N(N+1)/2$-dimensional simultaneous equations. In addition, Eq. (10) can be decomposed into N^2 equations. The solution of Eq. (10) is rewritten as a linear combination of the solutions of the these equations. In the special case when the stoichiometric matrix A is decouplable, this decomposition is significantly simplified into a linear combination of no more than N terms rather than N^2 terms. These terms can be considered as representations of all the noise components that originate from different noise sources (see Appendices A and B for detail).

In summary, one can obtain the covariance matrix of the stable distribution around a deterministic stable equilibrium point by taking the following steps:

1. Find two matrices, the stoichiometric matrix A and the propensity function $\boldsymbol{W}(\boldsymbol{X})$ of the system to be considered.
2. Find a stable equilibrium point $\boldsymbol{\phi} = \boldsymbol{\phi}^{eq}$ of Eq. (6).
3. Calculate two matrices $K(\boldsymbol{\phi}^{eq})$ and $D(\Omega\boldsymbol{\phi}^{eq})$.
4. Solve the Lyapunov equation (10).

Note that the derivation shown above, though simple, gives the same result as the original derivation (van Kampen, 1992) for the first and the second order cumulants of a stationary distribution, and even for those cumulants of the transient distribution under the assumptions $\boldsymbol{\mathcal{E}} \sim O(\Omega^{1/2})$ and $\Omega \to \infty$ to eliminate the last term in Eq. (9).

2.2 Measure of Noise

We use the covariance matrix Σ itself as the measure of noise unless otherwise explicitly noted. Normalized covariance matrix Σ^0 is partly used, which is equivalent to the coefficient of variation (CV). The normalized covariance is defined as $\Sigma^0 = S\Sigma S^{\mathrm{T}}$, where matrix $S = \mathrm{diag}\left(1/\left(\Omega\phi_1^{eq}\right), 1/\left(\Omega\phi_2^{eq}\right), \ldots, 1/\left(\Omega\phi_N^{eq}\right)\right)$ denotes the normalization by the mean values, i.e., the deterministic equilibrium point.

Furthermore, we use the following characteristic values of the noise:

$$\begin{aligned} \eta_{max} \equiv \sqrt{\lambda_{max}} \quad &: \text{the maximum noise component,} \\ \boldsymbol{v}_{max} \quad &: \text{the maximum noise direction,} \end{aligned}$$

where λ_{max} and $\boldsymbol{v}_{max}$ denote the largest eigenvalue of Σ^0 and its eigenvector, respectively.

2.3 Representing Noise

Here, we make a note on the terms specially used in this paper to describe the two-dimensional distributions.

We use the term *in-phase direction* to denote the direction in which two random variables increase or decrease in phase with each other. Similarly, we use the term *anti-phase*

direction to denote the direction in which two random variables increase or decrease in anti-phase with each other.

We use *noise ellipsoids*, as shown in Figs. 1(b) and 1(d). The noise ellipsoids show the shapes of the Gaussian PDFs by their 1σ equiprobability curves.

Furthermore, we use *parameter space plots*, as shown in Figs. 1(c) and 2(c). These figures show the noise characteristics for various combinations of two parameters chosen as x- and y- axes. Solid curves represent the contour curves of the maximum noise component η_{max}, which we call the *equi-noise curves*. Each short arrow represents the maximum noise direction $\boldsymbol{v}_{max}$.

3 Results

3.1 Single-gene autoregulatory network

Let us consider a model of an autoregulatory gene, i.e., a gene that represses its own transcription. The noise reduction by autoregulation has been extensively studied both theoretically (Thattai & van Oudenaarden, 2001; Bundschuh *et al.*, 2003; Simpson *et al.*, 2003; Kobayashi & Aihara, 2003) and experimentally (Becskei & Serrano, 2000). However, since the expressed proteins often form dimers in solution and bind to the operator region as dimers (Ptashne, 1987), multivariate analysis is necessary.

This model consists of four reactions schematically illustrated in Fig. 1(a), namely, protein synthesis, dimerization, dissociation, and degradation. These reactions are represented as follows:

$$
\begin{aligned}
\emptyset &\xrightarrow{\alpha(x_2)g[n]} n\mathcal{P} \qquad (n = 0, 1, 2, \ldots), \\
2\mathcal{P} &\underset{k_d}{\overset{k_d K_d^{-1}}{\rightleftharpoons}} \mathcal{P}_2, \\
\mathcal{P} &\xrightarrow{k_r} \emptyset,
\end{aligned}
$$

where $\emptyset$ denotes the absence of effective molecular species; $\mathcal{P}$ and $\mathcal{P}_2$ denote the monomer and the dimer forms of the expressed proteins, respectively. The state variable $\boldsymbol{X} = (X_1, X_2)$ denotes the copy numbers of the total proteins and the dimers, respectively. This coordinate system is chosen so that the stoichiometric matrix A is *decoupled*, i.e.,

each of the reaction channels changes only one state variable for a single firing as shown below (see Appendix B). For protein synthesis, we consider prokaryotic translation as a fast process through which proteins are released into the cytoplasm in sharp bursts according to a geometric distribution (Berg, 1978; McAdams & Arkin, 1997; Thattai & van Oudenaarden, 2001). The transcription initiation rate $\alpha(x_2)$ is a monotonically decreasing function of $x_2 \equiv X_2/\Omega$, the concentration of the dimers, because we assume that protein-DNA binding occurs in the dimer forms of the proteins. Therefore, the protein synthesis is modeled as a set of reactions that produces n proteins with rate $\alpha(x_2)g[n]$ for $n = 0, 1, 2, \ldots$, where $g[n] = B^n/(B+1)^{n+1} (n = 0, 1, 2, \ldots)$ denotes the PDF of the geometric distribution with average B (the average burst size).

The stoichiometric matrix A and the propensity function $\boldsymbol{W}(\boldsymbol{X})$ for this network are as follows:

$$A = \begin{pmatrix} n & -1 & 0 & 0 \\ 0 & 0 & 1 & -1 \end{pmatrix}, \tag{11}$$

$$\boldsymbol{W}(\boldsymbol{X}) = \begin{pmatrix} \Omega\alpha(X_2/\Omega)g[n] \\ k_r X_1 \\ \Omega^{-1}k_d\left((X_1 - 2X_2)(X_1 - 2X_2 - 1)\right)/K_d \\ k_d X_2 \end{pmatrix}.$$

The deterministic equation (6) is calculated as follows:

$$\frac{\mathrm{d}\phi_1}{\mathrm{d}t} = \alpha(\phi_2)B - k_r\phi_1, \tag{12}$$

$$\frac{\mathrm{d}\phi_2}{\mathrm{d}t} = k_d\Big\{\left(\phi_m(\phi_1,\phi_2)\left(\phi_m(\phi_1,\phi_2) - \Omega^{-1}\right)\right)/K_d - \phi_2\Big\}, \tag{13}$$

where $\phi_m(\phi_1, \phi_2) \equiv \phi_1 - 2\phi_2$ is the concentration of the monomers.

Furthermore, the matrices $K(\boldsymbol{\phi})$ and $D(\Omega\boldsymbol{\phi})$ are calculated as follows:

$$K(\boldsymbol{\phi}) = \begin{pmatrix} -k_r & \alpha'(\phi_2)B \\ k_d\left(2\phi_m - \Omega^{-1}\right)/K_d & -k_d\Big\{1 + 2\left(2\phi_m - \Omega^{-1}\right)/K_d\Big\} \end{pmatrix}, \tag{14}$$

$$D(\Omega\boldsymbol{\phi}) = \Omega\begin{pmatrix} k_r\Big\{\frac{\alpha(\phi_2)B}{k_r}(2B+1) + \phi_1\Big\} & 0 \\ 0 & k_d\Big\{\left(\phi_m\left(\phi_m - \Omega^{-1}\right)\right)/K_d + \phi_2\Big\} \end{pmatrix},$$

where $\alpha'(\phi_2) = \mathrm{d}\alpha/\mathrm{d}x_2|_{\phi_2}$. Here, summation over all n is taken and the relations $\sum_{n=0}^{\infty} ng[n] = B$ and $\sum_{n=0}^{\infty} n^2 g[n] = 2B^2 + B$ are used.

It can be shown that Eqs. (12) and (13) have the unique equilibrium point $\boldsymbol{\phi}^{eq} = (\phi_1^{eq}, \phi_2^{eq})^{\mathrm{T}}$ that is stable (see Appendix C.1). Therefore, we do not consider the whole function $\alpha(x_2)$, rather we consider two parameters $\alpha \equiv \alpha(\phi_2^{eq})$ and $\rho \equiv -\alpha'(\phi_2^{eq})B/k_r$. We call ρ the negative feedback strength, because here we consider only the autoregulatory network with $\alpha'(\phi_2^{eq}) < 0$.

Because D is a diagonal matrix, the solution of the Lyapunov equation (10) is decomposed into two noise components that originate from different noise sources (see Appendix A for detail). When the dimerization and the dissociation are much faster than the degradation ($k_{11}/k_{22} = k_r/(k_d\gamma) \ll 1$), the solution (Eq. (A.6)) is further reduced as follows:

$$\Sigma \simeq m_t \frac{1+B}{1+\rho\eta} \begin{bmatrix} 1 & \eta \\ \eta & \eta^2 \end{bmatrix} + m_d \gamma^{-1} \begin{bmatrix} \frac{\rho^2\kappa_{11}}{1+\rho\eta} & -\frac{\rho\kappa_{11}}{1+\rho\eta} \\ -\frac{\rho\kappa_{11}}{1+\rho\eta} & 1 \end{bmatrix}, \tag{15}$$

where,

$$\begin{aligned}
m_t &\equiv \Omega\phi_1^{eq} && : \text{the copy number of the total proteins at the equilibrium point,} \\
m_d &\equiv \Omega\phi_2^{eq} && : \text{the copy number of the dimers at the equilibrium point,} \\
\rho &\equiv k_{12}/k_{11} = -\alpha'(\phi_2^{eq})B/k_r && : \text{the negative feedback strength,} \\
\eta &\equiv -k_{21}/k_{22} = (2\phi_m^{eq} - \Omega^{-1})/(K_d + 2(2\phi_m^{eq} - \Omega^{-1})), \\
\gamma &\equiv -k_{22}/k_d = 1 + 2\,(2\phi_m^{eq} - \Omega^{-1})/\,K_d, \\
\kappa_{11} &\equiv k_{11}/(k_{11} + k_{22}) = k_r/\,(k_r + k_d\gamma)\,.
\end{aligned}$$

The first term of Eq. (15) represents the noise component generated by the protein synthesis and degradation, namely, the *protein birth and death noise*. The scalar part $m_t(1+B)/(1+\rho\eta)$ and the eigenvector $(1,\eta)^{\mathrm{T}}$ of the matrix part $(1,\eta)^{\mathrm{T}}(1,\eta)$ represent the magnitude and the direction of the fluctuation produced by this noise component, respectively. The second term of Eq. (15) represents the noise component generated by the monomer-dimer fluctuation, namely, the *monomer-dimer fluctuation noise*. The magnitude is $m_d\gamma^{-1}$, which is independent of the negative feedback strength ρ, and similarly, the direction of this noise component is represented by the 2×2 matrix multiplied from the right. The (2,2) component of this matrix is independent of the negative feedback

strength ρ and is dominant for small ρ. Therefore, the direction of this second noise component is approximately in the direction that changes the number of the dimers but holds the number of total proteins constant, which is denoted by $(0,1)^{\mathrm{T}}$.

Figure 1(b) shows the noise ellipsoids with four different values of the negative feedback strength ρ. All other parameter values are listed in Appendix D. Here, the negative feedback effectively represses the *protein birth and death noise* in the *in-phase direction* However, the *monomer-dimer fluctuation noise* in the *anti-phase direction* is not affected. This is clearly explained above in the analytical expression (Eq. (15)). The directions of the *protein birth and death noise* $(1,\eta)^{\mathrm{T}}$ (chained lines) and the directions of the *monomer-dimer fluctuation noise* $(0,1)^{\mathrm{T}}$ (dotted lines) are shown. For visualization, we transformed the two vectors in the $(X_1, X_2)^{\mathrm{T}}$ space into the normalized coordinate system of the copy numbers of the monomers and the dimers.

Figure 1(c) is the parameter space plot with the transcription initiation rate α and the negative feedback strength ρ as x- and y-axes, respectively. Here, in addition to the equi-noise curves, the direction of noise is shown as a short arrow for each pair of parameters. Increasing the negative feedback strength ρ reduces the maximum noise component η_{max} when ρ is below a certain value. However, there is a critical negative feedback strength above which η_{max} cannot further be reduced. Moreover, the maximum noise direction $\boldsymbol{v}_{max}$ changes from the *protein birth and death noise* (arrows pointing the upper right) to the *monomer-dimer fluctuation noise* (arrows pointing the upper left) at the critical value of ρ. Therefore, the autoregulation is effective in reducing the noise generated by protein synthesis and degradation, but not the noise generated by monomer-dimer fluctuation.

Figure 1(d) shows the noise ellipsoids for different values of the dimer dissociation constant K_d with the number of total proteins kept constant. The equilibrium point moves from low-monomers state to high-monomers state as K_d increases. The direction of the *protein birth and death noise* (chained line) changes from the dimer (upward) direction to the monomer (rightward) direction, but the direction of the *monomer-dimer fluctuation noise* (dotted line) is unchanged. When the fluctuation of the monomers is large, the fluctuation of the dimers is small, and vice versa. Therefore, there exists a trade-off between the fluctuation in monomers and that in dimers.

3.2 Two-gene autoregulatory network

Next, we present a simple example that the direction of noise in a genetic network can be controlled by changing the network parameters.

Let us consider a model of an autoregulatory network of two genes. This network, illustrated in Fig. 2(a), consists of two protein species $\mathcal{A}$ and $\mathcal{B}$, and two genes *gene a* and *gene b* coding the proteins, respectively. Here, we assume that protein $\mathcal{A}$ represses the transcription of *gene b*, while protein $\mathcal{B}$ activates the transcription of *gene a*. For simplicity, we omit dimerization and regard protein monomer molecules to be responsible for transcription regulation. Thus, this model consists of two variables X_1 and X_2, namely, the copy numbers of protein species $\mathcal{A}$ and $\mathcal{B}$, respectively, and four reactions, namely, syntheses and degradations of $\mathcal{A}$ and $\mathcal{B}$. These reactions can be represented as follows:

$$
\begin{aligned}
\emptyset &\xrightarrow{\alpha(x_2)g_1[n]} n\mathcal{A} \qquad (n = 0, 1, 2, \ldots), \\
\mathcal{A} &\xrightarrow{k_{r1}} \emptyset, \\
\emptyset &\xrightarrow{\beta(x_1)g_2[n']} n'\mathcal{B} \qquad (n' = 0, 1, 2, \ldots), \\
\mathcal{B} &\xrightarrow{k_{r2}} \emptyset,
\end{aligned}
$$

The stoichiometric matrix A and the propensity function $\boldsymbol{W}(\boldsymbol{X})$ are as follows:

$$
A = \begin{pmatrix} n & -1 & 0 & 0 \\ 0 & 0 & n' & -1 \end{pmatrix}, \qquad \boldsymbol{W}(\boldsymbol{X}) = \begin{pmatrix} \Omega\alpha(X_2/\Omega)g_1[n] \\ k_{r1}X_1 \\ \Omega\beta(X_1/\Omega)g_2[n'] \\ k_{r2}X_2 \end{pmatrix}. \tag{16}
$$

Accordingly, the deterministic equation (6) is calculated as follows:

$$
\frac{\mathrm{d}\phi_1}{\mathrm{d}t} = \alpha(\phi_2)B_1 - k_{r1}\phi_1, \tag{17}
$$

$$
\frac{\mathrm{d}\phi_2}{\mathrm{d}t} = \beta(\phi_1)B_2 - k_{r2}\phi_2, \tag{18}
$$

where B_1 and B_2 denote the average numbers of protein molecules synthesized from mRNAs (the average burst size) for the two genes, respectively.

Furthermore, the matrices $K(\boldsymbol{\phi})$ and $D(\Omega\boldsymbol{\phi})$ are calculated as follows:

$$
\begin{aligned}
K(\boldsymbol{\phi}) &= \begin{pmatrix} -k_{r1} & \alpha'(\phi_2)B_1 \\ \beta'(\phi_1)B_2 & -k_{r2} \end{pmatrix}, \\
D(\Omega\boldsymbol{\phi}) &= \Omega \begin{pmatrix} k_{r1}\left(\frac{\alpha(\phi_2)B_1}{k_{r1}}(2B_1+1)+\phi_1\right) & 0 \\ 0 & k_{r2}\left(\frac{\beta(\phi_1)B_2}{k_{r2}}(2B_2+1)+\phi_2\right) \end{pmatrix},
\end{aligned}
\tag{19}
$$

where $\alpha'(\phi_2) \equiv \mathrm{d}\alpha/\mathrm{d}x_2|_{x_2=\phi_2}$ and $\beta'(\phi_1) \equiv \mathrm{d}\beta/\mathrm{d}x_1|_{x_1=\phi_1}$.

It can be shown that Eqs. (17) and (18) have the unique equilibrium point $\boldsymbol{\phi}^{eq} = (\phi_1^{eq}, \phi_2^{eq})^{\mathrm{T}}$ that is stable, because protein $\mathcal{A}$ regulates protein $\mathcal{B}$ negatively, and protein $\mathcal{B}$ regulates protein $\mathcal{A}$ positively (see Appendix C.2). Therefore, similarly to the single gene case, we use four parameters $\alpha \equiv \alpha(\phi_2^{eq})$, $\rho_\alpha \equiv \alpha'(\phi_2^{eq})B_1/k_{r1}$, $\beta \equiv \beta(\phi_1^{eq})$, and $\rho_\beta \equiv -\beta'(\phi_1^{eq})B_2/k_{r2}$. We call ρ_α and ρ_β the positive and the negative regulatory strength, respectively.

Because D is a diagonal matrix, the solution of the Lyapunov equation (10) is decomposed into two noise components, namely, the protein $\mathcal{A}$ noise and the protein $\mathcal{B}$ noise, which are generated by the syntheses and degradations of these two protein species. For the case when the degradation rate constants of the two genes are equal $k_{r1} = k_{r2}$, the solution (Eq. (A.6)) is further reduced as follows:

$$
\begin{aligned}
\Sigma = &\frac{1}{2}m_1(1+B_1)\left[\begin{pmatrix} 1 & 0 \\ 0 & 0 \end{pmatrix} + \frac{1}{1+\rho_\alpha\rho_\beta}\begin{pmatrix} 1 & -\rho_\beta \\ -\rho_\beta & \rho_\beta^2 \end{pmatrix}\right] \\
&+ \frac{1}{2}m_2(1+B_2)\left[\begin{pmatrix} 0 & 0 \\ 0 & 1 \end{pmatrix} + \frac{1}{1+\rho_\alpha\rho_\beta}\begin{pmatrix} \rho_\alpha^2 & \rho_\alpha \\ \rho_\alpha & 1 \end{pmatrix}\right],
\end{aligned}
\tag{20}
$$

where $m_1 \equiv \Omega\phi_1^{eq}$ and $m_2 \equiv \Omega\phi_2^{eq}$. Here, note that $(1, -\rho_\beta)^{\mathrm{T}}$ or $(\rho_\alpha, 1)^{\mathrm{T}}$ becomes approximately the eigenvector of each term when one of the regulation is much stronger than the other, i.e., $\rho_\beta \gg \rho_\alpha$ or $\rho_\alpha \gg \rho_\beta$, respectively, and the product of them is small $\rho_\alpha\rho_\beta \ll 1$.

Figure 2(b) shows the noise ellipsoids for different values of the positive ρ_α or the negative ρ_β regulation. All other parameter values are listed in Appendix D. The distribution is spherically symmetric without the regulations. The positive regulation makes the distribution correlated to the *in-phase direction*. On the other hand, the negative regulation makes the distribution correlated to the *anti-phase direction*. These results demonstrate

that the direction of the noise in this network can be controlled in the opposite way by changing the strength of positive or negative regulation.

Figure 2(c) is the parameter space plot that shows this change more clearly. When the positive and the negative regulatory strengths are equal ($\rho_\alpha = \rho_\beta$, on the diagonal line), the distribution is symmetric, in other words, has no correlation. However, when $\rho_\alpha > \rho_\beta$, the distribution becomes correlated to the *in-phase direction* and vice versa. When ρ_α and ρ_β are small, the change in the direction of noise is smooth. However, when they are large, the change across the diagonal line of Fig. 2(c) is abrupt. This implies that a small change in parameter values in this region can drastically change the phenotypic noise characteristics.

To explain these observations, we set the transcription initiation rates $\alpha = \beta$ and the average burst sizes $B_1 = B_2$, according to the parameters used for the above calculations. Now, Eq. (20) is reduced as follows:

$$\frac{1}{2}m(1+B)\begin{pmatrix} 1+\frac{1+\rho_\alpha^2}{1+\rho_\alpha\rho_\beta} & \frac{\rho_\alpha-\rho_\beta}{1+\rho_\alpha\rho_\beta} \\ \frac{\rho_\alpha-\rho_\beta}{1+\rho_\alpha\rho_\beta} & 1+\frac{1+\rho_\beta^2}{1+\rho_\alpha\rho_\beta} \end{pmatrix}, \tag{21}$$

where $m \equiv m_1 = m_2$, and $B \equiv B_1 = B_2$.

The change in the direction of noise across the diagonal line is explained by the fact that the sign of the covariance is determined by the difference of ρ_α from ρ_β. In addition, two terms, $(1+\rho_\alpha^2)/(1+\rho_\alpha\rho_\beta)$ and $(1+\rho_\beta^2)/(1+\rho_\alpha\rho_\beta)$ in Eq. (21) explain the abrupt change in the direction of noise. These two terms can be rewritten as $(1+ar)/(1+a)$ where $a = \rho_\alpha\rho_\beta$ and $r = \rho_\alpha/\rho_\beta$ (or $r = \rho_\beta/\rho_\alpha$ for the latter term) are the product and the ratio of the two parameters. r denotes the deviation from the diagonal line. The coefficient $a/(1+a)$ denotes the sensitivity of that change in the $(1,1)$ or $(2,2)$ element of Eq. (21) produced by the change in r; this coefficient becomes large as a increases. Therefore, in the region of large a, the direction of the maximum eigenvector of the covariance matrix (Eq. (21)) changes to the rightward direction ($\rho_\alpha > \rho_\beta$) or to the upward direction ($\rho_\alpha < \rho_\beta$) as soon as the parameters deviate from the diagonal line.

3.3 A Biologically plausible model of the two-gene autoregulatory network

We consider the biologically plausible model of the two-gene autoregulatory network schematically illustrated in Fig. 3(a). It incorporates the *E. coli lacI* gene and the Ptrc-2 promoter as the repressive regulatory pair, and the bacteriophage λ *cI* gene and the P_{RM} promoter with mutant operator O_R3^- as the activatory regulatory pair, in which CI cannot repress its own transcription (Ptashne, 1987). Here, the functions $\alpha(x_2)$ and $\beta(x_1)$ in Eq. (16) are modeled by Hill functions as follows:

$$\alpha(x_2) = \frac{\alpha_0 (x_2/K_\alpha)^{h_\alpha}}{1 + (x_2/K_\alpha)^{h_\alpha}}, \tag{22}$$

$$\beta(x_1) = \frac{\beta_0}{1 + (\frac{x_1}{1+([\mathrm{IPTG}]/K_I)^{h_I}}/K_\beta)^{h_\beta}}, \tag{23}$$

where, $x_1 \equiv X_1/\Omega$ and $x_2 \equiv X_2/\Omega$ denote the concentrations of LacI and CI proteins, respectively. Here, isopropyl-β-thiogalactopyranoside (IPTG), which inactivates LacI repressor, is incorporated in order to control the repression of the Ptrc-2 promoter by LacI (Gardner *et al.*, 2000).

Figure 3(b) shows the noise ellipsoids for different concentrations of IPTG at deterministic equilibrium points. The equilibrium point moves from a low to a high copy number state as the IPTG concentration increases. Meanwhile, the direction of the noise around the equilibrium point changes from the *in-phase direction* to the *anti-phase direction*. This is more clearly shown in Fig. 3(c). This can be explained as follows. The gradient of the positive regulatory function $\alpha(x_2)$ at the equilibrium point is large at low IPTG concentrations and becomes small as IPTG increases, while the gradient of the negative regulatory function $\beta(x_1)$ is not so much affected. Therefore, $\rho_\alpha > \rho_\beta$ holds at low IPTG concentrations and $\rho_\beta > \rho_\alpha$ holds at high IPTG concentrations.

We note that the analytical results are in good correspondence with the stochastic simulation of the detailed model (see the noise ellipsoids in broken lines of Fig. 3(b), see Appendix E for detail).

3.4 Mutually repressive switch

As the last model, we consider the mutually repressive two-gene network schematically illustrated in Fig. 4(a). This kind of networks have been extensively studied, and shown both theoretically (Wolf & Eeckman, 1998; Cherry & Adler, 2000; Gardner *et al.*, 2000) and experimentally (Gardner *et al.*, 2000; Ozbudak *et al.*, 2004) that it can be monostable or bi-stable with hysteresis depending on parameter values that can be externally controlled. In other words, it can function as a genetic toggle switch. Here, we aim to shed light on the stochastic nature of the bifurcation phenomenon in the genetic switch, which has been conventionally analyzed deterministically. In addition, we test the validity of applying our analytical method to each equilibrium point independently in multistable systems.

In this model, the *E. coli lacI* gene and the Ptrc-2 promoter pair, and the bacteriophage λ *cI* gene and the $\mathrm{P_L}$ promoter pair are incorporated to produce mutual repression. IPTG is also incorporated to control the repression of the Ptrc-2 promoter by LacI.

We model mutual repression by setting both $\alpha(x_2)$ and $\beta(x_1)$ in Eq. (16) as monotonically decreasing functions as follows (Gardner *et al.*, 2000):

$$\alpha(x_2) = \frac{\alpha_0}{1 + (x_2/K_\alpha)^{h_\alpha}}, \tag{24}$$

$$\beta(x_1) = \frac{\beta_0}{1 + (\frac{x_1}{1+([\mathrm{IPTG}]/K_I)^{h_I}}/K_\beta)^{h_\beta}}, \tag{25}$$

where, $x_1 \equiv X_1/\Omega$ and $x_2 \equiv X_2/\Omega$ denote the concentrations of LacI and CI proteins, respectively.

Figure 4(b) shows the noise ellipsoids for different concentrations of IPTG at deterministic stable equilibrium points. As the negative regulation of Ptrc-2 by LacI is relaxed by the IPTG induction, the lower-right equilibrium point with high LacI and low CI disappears through saddle-node bifurcation, however the upper-left equilibrium point with low LacI and high CI remains stable. Applying the LNA to each stable equilibrium point gives us further information. We can see that the noise around the lower-right equilibrium point grows rapidly as the IPTG concentration increases. The noise ellipsoids cover the saddle point before the deterministic bifurcation occurs. On the other hand, noise around the upper-left equilibrium point is almost unchanged during the IPTG induction.

We note that the analytical results are practically in good correspondence with the stochastic simulations of the detailed model. The comparisons are shown Appendix E.

3.5 Summary of results

In this section, we have applied the LNA of the CME along with the decoupling of a stoichiometric matrix (see the discussions in the next section and Appendix B) to three fundamental types of genetic regulatory networks, that is, a single-gene autoregulatory network, a two-gene autoregulatory network, and a mutually repressive network.

In the single-gene autoregulatory network, we have found that there exist two differently originating noise components, namely, the *protein birth and death noise* and the *monomer-dimer fluctuation noise*. Each of them has its own characteristic magnitude and direction. The autoregulation is effective in reducing the former noise component but not the latter. Additionally, we have found that the dimer dissociation constant K_d determines not only the distribution of proteins between monomers and dimers but also the distribution of noise between the fluctuations of the monomers and dimers. This result has been clearly shown as the change in the *direction of noise* from the dimer direction to the monomer direction.

Next, we focused on the mechanism that changes the direction of noise. We investigated a two-gene autoregulatory network. We have shown that the direction of noise can be controlled drastically by changing the balance between the positive regulation and the negative regulation. Furthermore, with a biologically plausible two-gene autoregulatory network consisting of the *lacI* gene and the *cI* gene, we have shown that the direction of the noise around the equilibrium point changes from the in-phase direction to the anti-phase direction by the IPTG induction.

Finally, we have applied our method to a two-gene toggle-switch network. We have evaluated the stochastic fluctuations around the two equilibrium points in the genetic switch under the IPTG induction. We have found that while deterministically one of the two stable equilibrium points disappears through the saddle-node bifurcation, the noise around the disappearing equilibrium point grows rapidly. The noise ellipsoid covers the saddle point before the deterministic bifurcation occurs. On the other hand, the noise around the remaining equilibrium point is almost unchanged during the IPTG induction.

4 Discussion and Conclusion

4.1 LNA in the analysis of noise in genetic regulatory networks

In spite of the intrinsic nature of noise in genetic regulatory networks, the diversities of the copy numbers and the time scales among the molecular species have been keeping both numerical and analytical analyses of the noise difficult. In this paper, we have used the LNA of the CME for the noise analysis, which was originally proposed in (van Kampen, 1992). It is an analytical method that can evaluate stochastic fluctuations around deterministic stable equilibrium points. It is rigorously derived from the CME and can be systematically applied to arbitrary N-dimensional problems. One needs only to (i) find the stoichiometric matrix A and the propensity function $\boldsymbol{W}(\boldsymbol{X})$, (ii) find a stable equilibrium point of Eq. (6), (iii) calculate two matrices K and D there, and (iv) solve the Lyapunov equation (10). Here, we emphasize that no manipulation of the CME is necessary when we utilize this method.

We remark that the LNA has two different impacts. The first point is that it enables us to make a quick and accurate estimation of the PDF in arbitrary N-dimensional problems. This has been pointed out and emphasized in the previous study (Elf *et al.*, 2003; Elf & Ehrenberg, 2003) that applied the LNA to near-critical phenomena in biochemically reacting systems. This factor is important for the lack of an efficient numerical method that is generally and systematically applicable to arbitrary N-dimensional problems. However, mere numerical calculation gives little insight into the mechanisms behind the evaluated fluctuation and hardly improve our understanding of intracellular phenomena. Additionally, it should be noted that the cumulant evolution equation can improve the accuracy of the calculation with almost the same computational cost (Kobayashi & Aihara, 2003).

The second and the most important point is that it enables us to obtain the analytical representation of a covariance matrix, which preserves the full parameter dependence. This analytical representation is usually intractably complicated. Therefore, we have proposed the decoupling of a stoichiometric matrix in advance to the LNA.

The decoupling of a stoichiometric matrix A is a transformation of variables that guarantees that each of the reaction channels changes only one variable for a single firing. If such a transformation of variables exist, i.e., A is *decouplable*, the diffusion matrix D (defined as Eq. (5)) is diagonalized, and the representation of the covariance matrix is

decomposed into a linear combination of N different noise components as follows:

$$\Sigma = \sum_{i=1}^{N} \nu_{ii} M^{(i,i)}, \tag{26}$$

where $\nu_{ii} \equiv d_{ii}(\boldsymbol{\phi}^{eq})/(-2k_{ii}(\boldsymbol{\phi}^{eq}))$ represents the magnitude of the i-th noise component and $M^{(i,i)}$, which is a positive semidefinite matrix, represents the characteristic dispersion produced by the i-th noise component. Therefore, we call the maximum eigenvector of $M^{(i,i)}$ the *direction* of the i-th noise component (see Appendix A for detail).

The decoupling of a stoichiometric matrix significantly simplifies the representation of a covariance matrix into a set of N distinct noise components, rather than a single $N \times N$ covariance matrix. Therefore, it extends the power of the LNA from the quick evaluation of fluctuation to an understanding of the mechanisms behind such fluctuation.

4.2 Diagonalization of K or D

In the previous study (Elf & Ehrenberg, 2003) the diagonalization of K was used with the LNA.

Both the diagonalization of K and D are transformations of variables. Because the diagonalization of K elucidates the time scale of the dynamics, it has great importance in the deterministic dynamical systems analysis. On the other hand, the diagonalization of D has two remarkable points, which are especially important in the stochastic analysis.

The first point is that it removes the second order correlations of those probabilistic jumps in the copy numbers which are produced by randomly occurring reactions. This is explained as follows. The diffusion matrix D can be defined as the second order jump moment (van Kampen, 1992) as follows:

$$\begin{aligned} D\left(\boldsymbol{X}(t)\right) &\equiv \left\{ \lim_{\Delta t \to 0} \frac{\left\langle \left(\mathcal{X}_i(t+\Delta t) - X_i(t)\right)\left(\mathcal{X}_j(t+\Delta t) - X_j(t)\right)\right\rangle}{\Delta t} \right\}_{ij} \\ &= \left\{ \lim_{\Delta t \to 0} \frac{\sum_{k=1}^{M} a_{ik} a_{jk} W_k\left(\boldsymbol{X}(t)\right)\Delta t + O(\Delta t^2)}{\Delta t} \right\}_{ij} \\ &= \left\{ \sum_{k=1}^{M} a_{ik} a_{jk} W_k\left(\boldsymbol{X}(t)\right) \right\}_{ij}, \end{aligned}$$

where $\mathcal{X}_i(t+\Delta t)\ (i = 1, \ldots, N)$ is the random variable that denotes the copy number of the molecular species S_i at time $t + \Delta t$ conditional on the copy number $X_i(t)$ at time t. Here,

the second order central jump moment, i.e., the covariance, can be similarly defined and is equal to D because the product $\langle \mathcal{X}_i(t+\Delta t) - X_i(t) \rangle \langle \mathcal{X}_j(t+\Delta t) - X_j(t) \rangle$ is $O(\Delta t^2)$. Thus, the diagonalization of D removes the second order correlations of the jumps.

The second point is the distinction between the stoichiometry represented by A and the kinetics represented by $\boldsymbol{W}(\boldsymbol{X})$. If there exists a transformation of variables that decouples a stoichiometric matrix A, i.e., A is decouplable, this transformation diagonalizes D, as mentioned in the previous section. Therefore, the diagonalization of D is possible independently of the kinetics $\boldsymbol{W}(\boldsymbol{X})$ when A is decouplable. Although, because of the positive definiteness of D, a transformation of variables that diagonalizes D also exists even when A is not decouplable, it depends not only on the stoichiometry A but also the kinetics $\boldsymbol{W}(\boldsymbol{X})$. Therefore, we do not consider such case. We note that the importance of this distinction has been phenomenologically recognized as the burst size effect (Thattai & van Oudenaarden, 2001; Ozbudak *et al.*, 2002) and has been clearly pointed out in (Elf & Ehrenberg, 2003).

4.3 The decomposition of noise into intrinsic and extrinsic noise components

The decomposition of noise into intrinsic and extrinsic noise components (Elowitz *et al.*, 2002; Swain *et al.*, 2002; Paulsson, 2004) can be considered as the special case of the decomposition of noise proposed in this paper (see Appendix A for detail). However, the motivations seems to be greatly different.

The decomposition proposed in (Paulsson, 2004) is motivated by the experimental study (Elowitz *et al.*, 2002) where the question was how much of the observed noise arises from the network under consideration (intrinsic noise) and how much is caused by the fluctuation of the molecular species outside of it (extrinsic noise). Therefore, only the action of the extrinsic variable to the intrinsic variable was considered and the action in the opposite direction was omitted (Paulsson, 2004). Additionally, the covariance of the two variables were omitted and only the variance of the intrinsic variable was used as the measure of noise.

On the other hand, the decomposition (Eq. (26)) proposed in this paper aims to simplify the solution of the Lyapunov equation (10). In general, there is no reason to consider some molecular species as more significant than the others without any a priori

knowledge. Thus, we did not concentrate on specific pathways but considered all the molecular species and reaction channels as equally significant. Therefore, $M^{(i,i)}$ of each decomposed noise component reflects the overall connections of the network.

Moreover, in section 3, we have shown that the direction of noise is important even in understanding the mechanisms behind the fluctuation of each molecular species independently. Therefore, the decomposition of noise (Eq. (26)) is a key to gain deep insight into these mechanisms.

4.4 Biological implications

4.4.1 Protein birth and death noise

The first term of Eq. (15), namely, the *protein birth and death noise*, can be regarded as the natural extension of (Thattai & van Oudenaarden, 2001) to a multivariate system. The scalar part is proportional to the total number of proteins m_t. The coefficient of this proportionality is $1 + B$ in the absence of autoregulation; it decreases as the negative feedback strength ρ increases. Furthermore, the 2×2 matrix $(1, \eta)(1, \eta)^{\mathrm{T}}$ multiplied to the scalar part represents how this noise is distributed between the fluctuations of the monomers and dimers.

4.4.2 Reducing noise by changing the direction of noise

The reduction of noise by homodimer formation (Bundschuh *et al.*, 2003) and heterodimer formation (Morishita & Aihara, 2004) previously analyzed employ essentially the same mechanism with the change in the direction of noise (Fig. 1(d)) in the single-gene autoregulatory network of this paper. The mechanism, in our words, changes the direction of noise from one of the molecular species, e.g., monomers, to the others, e.g., dimers. Indeed, the direction of the protein birth and death noise $(1, \eta)^{\mathrm{T}}$ is determined by the dimer dissociation constant K_d, which was shown to change greatly the effectiveness of reducing noise in (Bundschuh *et al.*, 2003). In other words, those mechanisms change the distribution of noise between molecular species tightly coupled in the stoichiometry. Our decoupling approach has worked well by taking an appropriate coordinate system that decouples the stoichiometric matrix and decomposes the noise into the *protein birth and death noise* and the *monomer-dimer fluctuation* noise.

4.4.3 Noise in synthetic genetic regulatory networks

The multivariate analysis enables us to estimate quantitatively the stochastic fluctuation around equilibrium points in multi-stable networks. It gives us a clear criterion to design a feasible genetic switch (Cherry & Adler, 2000; Kobayashi *et al.*, 2003) that can operate reliably even in low copy numbers. This is important because a synthetic network that require high copy numbers of the molecular species in order to operate reliably might disrupt the homeostasis of the host cell into which it is transformed.

4.5 Future directions

Recent advance in measurement technologies and accumulation in experimental data are increasing the need of multivariate analysis. However, mere numerical calculation technics lack the ability to improve our understandings of the mechanisms or the structures behind specific observations. We have proposed the use of the LNA along with the systematic decoupling of a stoichiometric matrix. The decoupling of a stoichiometric matrix is clearly suited for the analysis of the multivariate stochasticity in a large scale biochemical system because it simplifies the solution of the Lyapunov equation and facilitates analytical treatment. This method can be used to understand the fundamental structures that generate, enhance, or reduce the noise and to reveal not only how organisms can fight against the noise but also how they can utilize it. Furthermore, the trade-off between the fluctuations of multiple molecular species may be the key to understand the evolutionary advantages that have led real networks inside the organisms to such structures. These theoretical predictions could be confirmed by carefully designed experiments based on these predictions. The understanding of the mechanisms is also essential in such experiments. An analytical method, such as the one presented here, can provide a quick and accurate prediction over a range of parameters. They might accelerate the process from modelings to experiments, thus provide more hypotheses with opportunity to be tested.

Acknowledgments

The authors thank Dr. Hiroyuki Okano, Mr. Yoshihiro Morishita, and Dr. Yoh Iwasa for their helpful discussions and comments. The authors also acknowledge the valuable comments of the anonymous reviewers that greatly improved this paper. This study is

partially supported by Grant-in-Aid No.12208004 and by the Superrobust Computation Project in 21st Century COE Program on Information Science and Technology Strategic Core from the Ministry of Education, Culture, Sports, Science,and Technology, the Japanese Government.

References

Alberts, B., Johnson, A., Lewis, J., Raff, M., Roberts, K. & Walter, P. (2002). *Molecular Biology of the Cell.* Garland Publishing. 4th edition.

Arkin, A., Ross, J. & McAdams, H. H. (1998). Stochastic Kinetic Analysis of Developmental Pathway Bifurcation in Phage λ-infected *Escherichia coli* Cells. *Genetics,* **149**, 1633–1648.

Becskei, A. & Serrano, L. (2000). Engineering stability in gene networks by autoregulation. *Nature,* **405**, 590–593.

Berg, O. G. (1978). A Model for the Statistical Fluctuations of Protein Numbers in a Microbial Population. *J. Theor. Biol.* **71**, 587–603.

Blake, W. J., Kærn, M., Cantor, C. R. & Collins, J. J. (2003). Noise in eukaryotic gene expression. *Nature,* **422**, 633–637.

Bundschuh, R., Hayot, F. & Jayaprakash, C. (2003). The Role of Dimerization in Noise Reduction of Simple Genetic Networks. *J. Theor. Biol.* **220** (2), 261–269.

Cherry, J. L. & Adler, F. R. (2000). How to make a Biological Switch. *J. Theor. Biol.* **203** (2), 117–133.

Elf, J. & Ehrenberg, M. (2003). Fast Evaluation of Fluctuations in Biochemical Networks With the Linear Noise Approximation. *Genome Res.* **13**, 2475–2484.

Elf, J., Paulsson, J., Berg, O. G. & Ehrenberg, M. (2003). Near-Critical Phenomena in Intracellular Metabolite Pools. *Biophys. J.* **84**, 154–170.

Elowitz, M. B. & Leibler, S. (2000). A synthetic oscillatory network of transcriptional regulators. *Nature,* **403**, 335–338.

Elowitz, M. B., Levine, A. J., Siggia, E. D. & Swain, P. S. (2002). Stochastic Gene Expression in a Single Cell. *Science,* **297**, 1183–1186.

Gajić, Z. & Qureshi, M. T. J. (1995). *Lyapunov Matrix Equation in System Stability and Control.* Academic Press.

Gardner, T. S., Cantor, C. R. & Collins, J. J. (2000). Construction of a genetic toggle switch in *Escherichia coli. Nature,* **403**, 339–342.

Gibson, M. A. & Bruck, J. (2000). Efficient Exact Stochastic Simulation of Chemical Systems with Many Species and Many Channels. *J. Phys. Chem. A,* **104** (9), 1876–1889.

Gillespie, D. T. (1977). Exact Stochastic Simulation of Coupled Chemical Reactions. *J. Phys. Chem.* **81** (25), 2340–2361.

Gillespie, D. T. (2000). The chemical Langevin equation. *J. Chem. Phys.* **113** (1), 297–306.

Hasty, J., Pradines, J., Dolnik, M. & Collins, J. (2000). Noise-based switches and amplifiers for gene expression. *Proc. Natl. Acad. Sci. USA,* **97** (5), 2075–2080.

Houchmandzadeh, B., Wieschaus, E. & Leibler, S. (2002). Establishment of developmental precision and proportions in the early *Drosophila* embryo. *Nature,* **415**, 798–802.

Kepler, T. B. & Elston, T. C. (2001). Stochasticity in Transcriptional Regulation: Origins, Consequences, and Mathematical Representations. *Biophys. J.* **81** (6), 3116–3136.

Kobayashi, T. & Aihara, K. (2003). How Does Noise Propagate in Genetic Networks? A New Approach to Understand Stochasticity in Genetic Networks. *Proc. CEC 2003,* **2**, 1018–1025.

Kobayashi, T., Chen, L. & Aihara, K. (2003). Modeling Genetic Switches with Positive Feedback Loops. *J. Theor. Biol.* **221** (3), 379–399.

Lancaster, P. & Tismenetsky, M. (1985). *The Theory of Matrices.* Academic Press. 2nd edition.

McAdams, H. H. & Arkin, A. (1997). Stochastic mechanisms in gene expression. *Proc. Natl. Acad. Sci. USA,* **94**, 814–819.

Morishita, Y. & Aihara, K. (2004). Noise-Reduction through Interaction in Gene Expression and Biochemical Reaction Processes. *J. Theor. Biol.* . in press.

Ozbudak, E. M., Thattai, M., Kurtser, I., Grossman, A. D. & van Oudenaarden, A. (2002). Regulation of noise in the expression of a single gene. *Nat. Genet.* **31**, 69–73.

Ozbudak, E. M., Thattai, M., Lim, H. N., Shraiman, B. I. & Oudenaarden, A. V. (2004). Multistability in the lactose utilization network of Escherichia coli. *Nature,* **427**, 737–740.

Paulsson, J. (2004). Summing up the noise in gene networks. *Nature,* **427**, 415–418.

Peccoud, J. & Ycart, B. (1995). Markovian Modelling of Gene-Product Synthesis. *Theor. Popul. Biol.* **48** (2), 222–234.

Ptashne, M. (1987). *A Genetic Switch: Gene Control and Phage* λ. Blackwell Scientific Publications & Cell Press. 2nd edition.

Rao, C. V., Wolf, D. M. & Arkin, A. P. (2002). Control, exploitation and tolerance of intracellular noise. *Nature Insight,* **420**, 231–237.

Shea, M. A. & Ackers, G. K. (1985). The O_R Control System of Bacteriophage Lambda – A Physical-Chemical Model for Gene Regulation. *J.Mol. Biol.* **181**, 211–230.

Simpson, M. L., Cox, C. D. & Sayler, G. S. (2003). Frequency domain analysis of noise in autoregulated gene circuits. *Proc. Natl. Acad. Sci. USA,* **100** (8), 4551–4556.

Swain, P. S., Elowitz, M. B. & Siggia, E. D. (2002). Intrinsic and extrinsic contributions to stochasticity in gene expression. *Proc. Natl. Acad. Sci. USA,* **99** (20), 12795–12800.

Temkin, O. N., Zeigarnik, A. V. & Bonchev, D. (1996). *Chemical Reaction Networks: A Graph-Theoretical Approach.* CRC Press.

Thattai, M. & van Oudenaarden, A. (2001). Intrinsic noise in gene regulatory networks. *Proc. Natl. Acad. Sci. USA,* **98** (15), 8614–8619.

van Kampen, N. G. (1992). *Stochastic processes in physics and chemistry.* Elsevier Science, Amsterdam.

Wolf, D. M. & Eeckman, F. H. (1998). On the Relationship between Genomic Regulatory Element Organization and Gene Regulatory Dynamics. *J. Theor. Biol.* **195** (2), 167–186.

Appendix

A The solution of the Lyapunov equation and the decomposition of noise

In this section, we show that the solution of the Lyapunov equation (10) can be decomposed into $N \times N$ equations that do not include D, and the solution of the original Lyapunov equation (10) is written as a linear combination of the solutions of these equations. In addition, when D is diagonal, the solution is further simplified into a linear combination of N terms. Then, the decomposition of noise into its origins and the *directions* and *magnitudes* of noise are clearly defined.

We consider the following Lyapunov equation:

$$K\Sigma + \Sigma K^{\mathrm{T}} + D = 0, \tag{A.1}$$

where K is a $N \times N$ stable matrix and D is a positive semidefinite matrix of the same size.

Remark A.1 *The solution of Eq.* (A.1) *is unique and can be written explicitly as follows (Gajić & Qureshi, 1995):*

$$\Sigma = \int_0^\infty e^{Kt} D e^{K^{\mathrm{T}} t} \mathrm{d}t. \tag{A.2}$$

However, this representation is not suited for an analytical study. Therefore, we write the solution of Eq. (A.1) as follows:

$$\Sigma = \sum_{i=1}^{N} \sum_{j=1}^{N} \nu_{ij} M^{(i,j)}, \tag{A.3}$$

where $\nu_{ij} \equiv d_{ij}/(-(k_{ii} + k_{jj}))$, and $M^{(i,j)}$, which is a symmetric matrix, is the solution of the following equations:

$$K M^{(i,j)} + M^{(i,j)} K^{\mathrm{T}} - (k_{ii} + k_{jj}) \left\{ \frac{1}{2} (\boldsymbol{e}_i \boldsymbol{e}_j^{\mathrm{T}} + \boldsymbol{e}_j \boldsymbol{e}_i^{\mathrm{T}}) \right\} = 0 \qquad (i, j = 1, \ldots, N), \tag{A.4}$$

where $\{\boldsymbol{e}_1, \ldots, \boldsymbol{e}_N\}$ is the standard basis in $\mathbb{R}^N$. This is easily proven by taking a summation of the left hand side of Eq. (A.4) weighted by ν_{ij} for $i, j = 1, \ldots, N$. Here, note

that $M^{(i,j)} = M^{(j,i)}$ holds.

Let $N(N+1)/2$ dimensional vectors $\tilde{\boldsymbol{\sigma}}$ and $\tilde{\boldsymbol{d}}$ be $\tilde{\boldsymbol{\sigma}} = \mathfrak{V}(\Sigma) \equiv (\sigma_{11}, \ldots, \sigma_{1N}, \sigma_{22}, \ldots, \sigma_{2N}, \ldots, \sigma_{NN})^{\mathrm{T}} \in \mathbb{R}^{N(N+1)/2}$ and $\tilde{\boldsymbol{d}} \equiv (d_{11}, 2d_{12}, \ldots, 2d_{1N}, d_{22}, 2d_{23}, \ldots, 2d_{2N}, \ldots, d_{N-1,N-1}, 2d_{N-1,N}, d_{NN})^{\mathrm{T}} \in \mathbb{R}^{N(N+1)/2}$. The following $N(N+1)/2$ simultaneous equation that is equivalent to Eq. (A.1) does uniquely exist:

$$\tilde{K}\tilde{\boldsymbol{\sigma}} = -\tilde{\boldsymbol{d}}. \tag{A.5}$$

Moreover the coefficients $\tilde{K}$ can be algorithmically obtained (Gajić & Qureshi, 1995).

Remark A.2 *$M^{(i,j)}$ $(j \geq i)$ is equivalent to the p-th column vector of $(k_{ii} + k_{jj})\tilde{K}^{-1}$:*

$$M^{(i,j)} = \mathfrak{V}^{-1}\left(\left\{(k_{ii} + k_{jj})\tilde{K}^{-1}\right\}_{p\text{-}th\ column\ vector}\right),$$

where $p = (2N + 2 - i)(i - 1)/\,2 + (j - i + 1)$.

The proof is straightforward because the only nonzero component in the right hand side of Eq. (A.5) equivalent to Eq. (A.4) is the p-th component and is equal to $(k_{ii} + k_{jj})$.

When D is diagonal, the solution (Eq. (A.3)) can be written in a more meaningful manner:

$$\Sigma = \sum_{i=1}^{N} \nu_{ii} M^{(i,i)},$$

where $\nu_{ii}\,(= d_{ii}/(-2k_{ii}))$ is the solution of the following scalar Lyapunov equation:

$$k_{ii}\nu_{ii} + \nu_{ii}k_{ii} + d_{ii} = 0, \qquad (i = 1, \ldots, N).$$

Therefore, it is natural to call ν_{ii} the *magnitude* of the i-th noise component. On the other hand, $M^{(i,i)}$, which is now a positive semidefinite matrix, represents the characteristic dispersion produced by the i-th noise component. Therefore, we call the maximum eigenvector of $M^{(i,i)}$ the *direction* of the i-th noise component. Here, note that the direction of noise is not a "directed" notion, i.e., $\boldsymbol{v}$ and $-\boldsymbol{v}$ represent the same direction of noise.

The magnitude of noise ν_{ii} $(i = 1, \ldots, N)$ reflects only the characteristics of a small set of reactions. For example, for protein synthesis and degradation, $d_{ii} = 2k_r(1 + B)m$ and $k_{ii} = -k_r$ give $\nu_{ii} = (1 + B)m$, where k_r, B, and m are the degradation rate constant, the average protein synthesis from mRNA, and the number of proteins at the deterministic

equilibrium point. On the other hand, $M^{(i,i)}$ $(i = 1, \ldots, N)$ is independent of D and reflects the global connections of the network, represented by K, e.g., binding to the other proteins or genetic regulation, as shown in the main text.

The exact form of decomposed covariance matrix Σ for $N = 2$, with which we have dealt in the main text, is as follows:

$$\Sigma = \nu_{11}\frac{k_{11}}{k_{11}+k_{22}}\left\{\begin{pmatrix}1 & 0\\ 0 & 0\end{pmatrix} + \frac{1}{\Delta}\begin{pmatrix}k_{22}^2 & -k_{21}k_{22}\\ -k_{21}k_{22} & k_{21}^2\end{pmatrix}\right\} + \nu_{22}\frac{k_{22}}{k_{11}+k_{22}}\left\{\begin{pmatrix}0 & 0\\ 0 & 1\end{pmatrix} + \frac{1}{\Delta}\begin{pmatrix}k_{12}^2 & -k_{12}k_{11}\\ -k_{12}k_{11} & k_{11}^2\end{pmatrix}\right\}, \tag{A.6}$$

where $\Delta \equiv k_{11}k_{22} - k_{12}k_{21}$. Here, note that $(k_{22}, -k_{21})^{\mathrm{T}}$ and $(-k_{12}, k_{11})^{\mathrm{T}}$ are the eigenvectors of the second and the fourth terms, respectively.

Furthermore, we show two special cases. The first case is when the time scales of the two components are far apart ($k_{11}, k_{12} \ll k_{21}, k_{22}$), $M^{(1,1)}$ and $M^{(2,2)}$ can be reduced as follows:

$$M^{(1,1)} = \frac{k_{11}}{k_{11}+k_{22}}\frac{1}{\Delta}\begin{pmatrix}k_{22}^2 & -k_{21}k_{22}\\ -k_{21}k_{22} & k_{21}^2\end{pmatrix}, \qquad M^{(2,2)} = \begin{pmatrix}0 & 0\\ 0 & 1\end{pmatrix}.$$

Here, the maximum (and the only) eigenvectors of $M^{(1,1)}$ and $M^{(2,2)}$ is $(k_{22}, -k_{21})^{\mathrm{T}}$ and $(0, 1)^{\mathrm{T}}$, respectively. This approximation has been used for the single gene autoregulatory network in the main text.

The second case is when the interaction is unidirectional, $k_{12} = 0$, which is the same assumption as that used in (Paulsson, 2004). This gives the equivalent result as the previous study:

$$\Sigma = \begin{pmatrix}\nu_{11} & -\nu_{11}\frac{k_{21}}{k_{11}+k_{22}}\\ -\nu_{11}\frac{k_{21}}{k_{11}+k_{22}} & \nu_{22} + \nu_{11}\left(\frac{k_{21}}{k_{22}}\right)^2\frac{k_{22}}{k_{11}+k_{22}}\end{pmatrix}.$$

B Decoupling of a stoichiometric matrix

First, we define the *decoupled* stoichiometric matrix.

Definition B.1 *A stoichiometric matrix A is said to be decoupled if each column vector of A has only one nonzero component.*

When A is decoupled, each of the reaction channels changes only one variable for a single firing. Therefore, each reaction channel corresponds to a state variable.

Definition B.2 *A stoichiometric matrix A is said to be decouplable if there exist a regular matrix $T \in \mathbb{Z}^{N\times N}$ such that TA is decoupled.*

If A is *decouplable*, T is obtained by performing the Gaussian elimination on A (Lancaster & Tismenetsky, 1985).

As mentioned in the main text, the next fact is important.

Remark B.1 *The sufficient condition for the diffusion matrix D to be diagonal is that the stoichiometric matrix A is decoupled.*

The proof is straightforward from the definition (Eq. (5)). Additionally, we do not consider the unnecessary case, because though it is possible that $\sum_{k=1}^{M} a_{ik}a_{jk}W_k(\boldsymbol{X}) = 0 \quad (^{\forall} i \neq j)$ holds for a specific $\boldsymbol{W}(\boldsymbol{X})$, any perturbation in the rate constants or the state variable $\boldsymbol{X}$ can break this equality.

As a summary, given an arbitrary stoichiometric matrix A, if A is decouplable, there exist a transformation of variables that makes the diffusion matrix D diagonal, and the covariance matrix a linear combination of N terms, as shown in the previous section. The overall picture of our theory is schematically shown in Fig. B1.

Next, we present a necessary and sufficient condition for A to be decouplable. Let us define a subset of reactions $\mathcal{R}_0\,(\subseteq \mathcal{R} = \{\mathrm{R}_1, \ldots, \mathrm{R}_M\})$ of size $M_0\,(\leq M)$ and an $N \times M_0$ matrix A_0. $\mathcal{R}_0$ is defined as the maximum subset of reactions whose stoichiometric matrix A_0 consists of pairwise linearly independent column vectors. Therefore, the original stoichiometric matrix A can be rewritten as $A = (A_0, A_1)$ where $A_0 \in \mathbb{Z}^{N\times M_0}$ and $A_1 \in \mathbb{Z}^{N\times(M-M_0)}$. Here, for each column vector $\boldsymbol{a}_1$ of A_1, there exist a rational number s and a column vector $\boldsymbol{a}_0$ of A_0 that satisfies $\boldsymbol{a}_1 = s\boldsymbol{a}_0$, e.g., when $s = -1$ the reaction corresponding to $\boldsymbol{a}_1$ is the reverse reaction of that corresponding to $\boldsymbol{a}_0$.

Generally, the whole set of reactions $\mathcal{R}$ can be partitioned into equivalence classes under a equivalence relation of pairwise linear dependence. $\mathcal{R}_0$ is the set of class representatives of these equivalence classes. If $\mathcal{R}_0$ is linearly independent, each equivalence class of reaction channels can be made to correspond to a state variable. This is formally expressed as follows.

Theorem B.1 *A is decouplable if and only if A_0 has full column rank.*

Proof. Sufficiency: Because A_0 has full column rank, $M_0 \leq N$. Therefore, we can choose T as:

$$T = \begin{pmatrix} S\left(A_0^{\mathrm{T}} A_0\right)^{-1} A_0^{\mathrm{T}} \\ A_{0\perp}^{\mathrm{T}} \end{pmatrix},$$

where $S = \mathrm{diag}(s_1, \ldots, s_{M_0}) \in \mathbb{Z}^{M_0 \times M_0}$ is an appropriate diagonal matrix that makes T an integer matrix, and $A_{0\perp} \in \mathbb{Z}^{N \times (N - M_0)}$ is a basis of the orthogonal complement space of A_0.

Necessity: Any decoupled stoichiometric matrix $\tilde{A} = TA$ can be rewritten as:

$$\tilde{A} = \left(\tilde{A}_0,\, \tilde{A}_1\right),$$

where

$$\tilde{A}_0 = \begin{pmatrix} S \\ \mathbf{0} \end{pmatrix} \in \mathbb{Z}^{N \times M_0},$$

$S = \mathrm{diag}(s_1, \ldots, s_{M_0}) \in \mathbb{Z}^{M_0 \times M_0}$, and $\tilde{A}_1$ is similarly defined as A_1. Therefore, $A = T^{-1}\left(\tilde{A}_0,\, \tilde{A}_1\right)$. Clearly, the first M_0 columns of A have full column rank and for each column vector $\boldsymbol{a}_1$ of $T^{-1}\tilde{A}_1$, there exist a a column vector $\boldsymbol{a}_0$ of $T^{-1}\tilde{A}_0$ that is pairwise linearly dependent to $\boldsymbol{a}_1$. ■

For example, the following chemical system is decouplable:

$$\begin{aligned}
&\mathcal{A} \overset{\mathrm{R}_1}{\underset{}{\rightleftharpoons}} \mathcal{B}, \\
&\mathcal{C} \overset{\mathrm{R}_3}{\underset{\mathrm{R}_2}{\rightleftharpoons}} \mathcal{D}, \\
&\mathcal{B} + \mathcal{D} \overset{\mathrm{R}_5}{\longrightarrow} \mathcal{B}, \mathcal{D}, \mathcal{C} \overset{\mathrm{R}_4}{\longrightarrow} \emptyset,
\end{aligned} \qquad A = \begin{array}{c} \\ \mathcal{A} \\ \mathcal{B} \\ \mathcal{C} \\ \mathcal{D} \end{array} \begin{array}{c} \begin{array}{ccccc} \mathrm{R}_1 & \mathrm{R}_3 & \mathrm{R}_5 & \mathrm{R}_2 & \mathrm{R}_4 \end{array} \\ \left(\begin{array}{ccccc} -1 & 0 & 0 & 1 & 0 \\ 1 & 0 & -1 & -1 & 0 \\ 0 & -1 & 0 & 0 & 1 \\ 0 & 1 & -1 & 0 & -1 \end{array}\right) \end{array}. \tag{B.1}$$

The decoupled stoichiometric matrix $\tilde{A} = TA$ is obtained as follows:

$$\tilde{A} = \begin{array}{c} \\ \mathcal{A} \\ \mathcal{A}+\mathcal{B} \\ (\mathcal{A}+\mathcal{B})-\mathcal{D} \\ (\mathcal{A}+\mathcal{B})-(\mathcal{C}+\mathcal{D}) \end{array} \begin{array}{c} \begin{array}{ccccc} \mathrm{R}_1 & \mathrm{R}_3 & \mathrm{R}_5 & \mathrm{R}_2 & \mathrm{R}_4 \end{array} \\ \left(\begin{array}{ccc:cc} -1 & 0 & 0 & 1 & 0 \\ 0 & 0 & -1 & 0 & 0 \\ 0 & -1 & 0 & 0 & 1 \\ 0 & 0 & 0 & 0 & 0 \end{array}\right) \end{array}. \tag{B.2}$$

The correspondence between the equivalence classes of reaction channels and the molecular species is well described by a bipartite graph (Temkin *et al.*, 1996) of a decoupled stoichiometric matrix. The bipartite graphs of the original and the decoupled stoichiometric matrices are shown in Fig. B2.

The following chemical system is not decouplable.

$$\begin{array}{l} \mathcal{A} \underset{\mathrm{R}_2}{\overset{\mathrm{R}_1}{\rightleftharpoons}} \mathcal{B}, \\ \mathcal{B} \underset{\mathrm{R}_4}{\overset{\mathrm{R}_3}{\rightleftharpoons}} \mathcal{C}, \\ \mathcal{C} \underset{\mathrm{R}_6}{\overset{\mathrm{R}_5}{\rightleftharpoons}} \mathcal{A}, \end{array} \qquad A = \begin{array}{c} \\ \mathcal{A} \\ \mathcal{B} \\ \mathcal{C} \end{array} \begin{array}{c} \begin{array}{ccc} \mathrm{R}_1 & \mathrm{R}_3 & \mathrm{R}_5 \end{array} \\ \left(\begin{array}{ccc} -1 & 0 & 1 \\ 1 & -1 & 0 \\ 0 & 1 & -1 \end{array}\right) \end{array},$$

whose Gaussian elimination ends up in the following form:

$$A = \begin{array}{c} \\ \mathcal{A} \\ \mathcal{A}+\mathcal{B} \\ \mathcal{A}+\mathcal{B}+\mathcal{C} \end{array} \begin{array}{c} \begin{array}{ccc} \mathrm{R}_1 & \mathrm{R}_3 & \mathrm{R}_5 \end{array} \\ \left(\begin{array}{ccc} -1 & 0 & 1 \\ 0 & -1 & 1 \\ 0 & 0 & 0 \end{array}\right) \end{array},$$

where the reverse reactions R_2, R_4, and R_6 were omitted.

C Proof of the stability conditions

C.1 Single-gene autoregulatory network

We prove that the equilibrium point of Eqs. (12) and (13) is unique and the Jacobian $K(\boldsymbol{\phi})$ (Eq. (14)) is stable for all $\boldsymbol{\phi} = (\phi_1, \phi_2)^{\mathrm{T}}$. Here, we assume that there are more

than 0.5 molecules of monomers as an average, i.e., $2\Omega\phi_m - 1 > 0$. This is satisfied in all cases in this paper. In addition, we use $\alpha'(\phi_2) < 0$ for all ϕ_2, since we are considering an autoregulatory gene.

[**Uniqueness**] The equilibrium condition of Eqs. (12)=(13)=0 can be rewritten as follows:

$$\phi_m\left(\alpha(\phi_2)B/\,k_r, \phi_2\right)\left(\phi_m\left(\alpha(\phi_2)B/\,k_r, \phi_2\right) - \Omega^{-1}\right) = K_d\phi_2, \tag{C.1}$$

where $\phi_m(\phi_1, \phi_2) = \phi_1 - 2\phi_2$ is the concentration of the monomers. By differentiating the left-hand side of Eq. (C.1) with respect to ϕ_2, we obtain

$$\left(2\phi_m\left(\alpha(\phi_2)B/\,k_r, \phi_2\right) - \Omega^{-1}\right)\left(\alpha'(\phi_2)B/\,k_r - 2\right) < 0.$$

Thus, the solution of Eq. (C.1) is unique. ■

[**Stability**] The trace and the determinant of the matrix $K(\boldsymbol{\phi})$ satisfy the following inequalities:

$$\begin{aligned}
\mathrm{tr}[K(\boldsymbol{\phi})] &= -\left\{k_r + k_d\left(1 + 2\left(2\phi_m - \Omega^{-1}\right)/\,K_d\right)\right\} < 0, \\
\det[K(\boldsymbol{\phi})] &= k_d k_r\left\{1 + \left(2 - \alpha'(\phi_2)B/k_r\right)\left(2\phi_m - \Omega^{-1}\right)/\,K_d\right\} > 0.
\end{aligned}$$

The eigenvalues of $K(\boldsymbol{\phi})$ are the solutions of the following characteristic equation:

$$\lambda^2 - \mathrm{tr}[K(\boldsymbol{\phi})]\lambda + \det[K(\boldsymbol{\phi})] = 0.$$

Thus, both of the eigenvalues of $K(\boldsymbol{\phi})$ have negative real parts for all $\boldsymbol{\phi} = (\phi_1, \phi_2)^{\mathrm{T}}$. ■

C.2 Two-gene autoregulatory network

We prove that the equilibrium point of Eqs. (17) and (18) is unique and the Jacobian $K(\boldsymbol{\phi})$ (Eq. (19)) is stable for all $\boldsymbol{\phi} = (\phi_1, \phi_2)^{\mathrm{T}}$. Here, we use $\alpha'(\phi_2)\beta'(\phi_1) < 0$ for all $\boldsymbol{\phi} = (\phi_1, \phi_2)^{\mathrm{T}}$, considering that the protein $\mathcal{A}$ represses the gene b coding protein $\mathcal{B}$, and the protein $\mathcal{B}$ activates the gene a coding protein $\mathcal{A}$.

[**Uniqueness**] The equilibrium condition of Eqs. (17)=(18)=0 can be rewritten as follows:

$$\alpha(\beta(\phi_1)B_2/k_{r2})B_1/k_{r1} = \phi_1. \tag{C.2}$$

By differentiating the left-hand side of Eq. (C.2) with respect to ϕ_1, we obtain

$$\alpha'\left(\beta(\phi_1)B_2/k_{r2}\right)\beta'(\phi_1)B_1B_2/(k_{r1}k_{r2}) < 0.$$

Thus, the solution of Eq. (C.2) is unique. ■

[**Stability**] The trace and the determinant of the matrix $K(\boldsymbol{\phi})$ satisfy the following inequalities:

$$\begin{aligned}\mathrm{tr}[K(\boldsymbol{\phi})] &= -(k_{r1}+k_{r2}) < 0,\\ \det[K(\boldsymbol{\phi})] &= k_{r1}k_{r2} - \alpha'(\phi_2)\beta'(\phi_1)B_1B_2 > 0.\end{aligned}$$

Thus, both of the eigenvalues of $K(\boldsymbol{\phi})$ have negative real parts for all $\boldsymbol{\phi} = (\phi_1, \phi_2)^{\mathrm{T}}$. ■

D Parameter values

Tables D1, D2, and D3 show the parameter values we used for the single-gene autoregulatory network (in section 3.1), the two-gene autoregulatory network (in section 3.2), and the biologically plausible two-gene autoregulatory and mutually repressive networks (in sections 3.3 and 3.4). All the parameter values were held constant at these values unless explicitly noted. We fixed the cell volume at 1.66×10^{-15}(liters) to be consistent with the *Escherichia coli* cell volume $\sim 10^{-15}$(liters) (Alberts *et al.*, 2002), and to make mathematical treatment easy. That is, this makes 1 molecule/cell correspond to the 1nM concentration. The transcription initiation rate α, the average burst size B, and the dimer dissociation constant K_d were obtained from (Shea & Ackers, 1985), which were values measured for the bacteriophage λ *cI* gene and the CI protein. The dimerization rate k_d is obtained from (Arkin *et al.*, 1998). The protein degradation rate k_r was adjusted to yield a half life roughly equal to the *E. coli* cell cycle (40 min).

E Comparison of the analytical results and the stochastic simulations

We compare the results in sections 3.3 and 3.4 with detailed stochastic simulations composed of 12 variables and 19 reactions. We use the Next Reaction Method (Gibson &

Bruck, 2000), which is an efficient and exact stochastic simulation algorithm based on a Monte-Carlo method well known as the Gillespie method (Gillespie, 1977).

For the two-gene autoregulatory network in section 3.3, we model that the transcription of the LacI mRNA initiates only from the *lacI* gene whose promoter $\mathrm{P_{RM}}$ is bound by two copies of CI, which is denoted by $\mathrm{DLac_2}$, as follows:

$$\mathrm{DLac_2} \xrightarrow{k_5} \mathrm{DLac_2 + mLac},$$

where k_5 denotes the open complex formation rate constant. For the two-gene mutually repressive network in section 3.4, we model that the transcription of the LacI mRNA initiates only from the *lacI* gene whose promoter $\mathrm{P_L}$ is not bound, which is denoted by $\mathrm{DLac_0}$, as follows:

$$\mathrm{DLac_0} \xrightarrow{k_5} \mathrm{DLac_0 + mLac}.$$

All the other reactions are the same for the two networks as follows:

$$
\begin{aligned}
\mathrm{DLac_0 + CI} &\underset{k_2}{\overset{k_1}{\rightleftharpoons}} \mathrm{DLac_1}, \\
\mathrm{DLac_1 + CI} &\underset{k_4}{\overset{k_3}{\rightleftharpoons}} \mathrm{DLac_2}, \\
\mathrm{mLac} &\xrightarrow{k_6} \mathrm{mLac + Lac}, \\
\mathrm{mLac} &\xrightarrow{k_7} \emptyset, \\
\mathrm{Lac + IPTG} &\underset{k_9}{\overset{k_8}{\rightleftharpoons}} \mathrm{Lac = IPTG}, \\
\mathrm{Lac} &\xrightarrow{k_{10}} \emptyset, \\
\mathrm{Lac = IPTG} &\xrightarrow{k_{11}} \mathrm{IPTG}, \\
\mathrm{DCI_0 + Lac} &\underset{k_{13}}{\overset{k_{12}}{\rightleftharpoons}} \mathrm{DCI_1}, \\
\mathrm{DCI_1 + Lac} &\underset{k_{15}}{\overset{k_{14}}{\rightleftharpoons}} \mathrm{DCI_2}, \\
\mathrm{DCI_0} &\xrightarrow{k_{16}} \mathrm{DCI0 + mCI}, \\
\mathrm{mCI} &\xrightarrow{k_{17}} \mathrm{mCI + CI}, \\
\mathrm{mCI} &\xrightarrow{k_{18}} \emptyset, \\
\mathrm{CI} &\xrightarrow{k_{19}} \emptyset,
\end{aligned}
$$

where $\mathrm{DLac}_i\,(i = 0, 1, 2)$ denotes the *lacI* gene whose promoter $\mathrm{P_{RM}}$ bound by i copies of CI; mLac, LacI, and LacI=IPTG denote the LacI mRNA, the LacI protein, and the LacI protein bound by IPTG, respectively. DCI_i, mCI, and CI are similarly used. All the values of the rate constants k_i are listed in Table E1.

E.1 Autoregulatory network

The comparisons between the LNA and the stochastic simulation are shown for two parameters: [IPTG]=16μM in Fig. E1 and [IPTG]=252μM in Fig. E2. The initial values of all the sample paths are set at the deterministic equilibrium point for each parameter; the number of the sample paths is 4000 and the length of each path is 20000s. Here, the axis, LacI denotes the sum of the IPTG bound and unbound LacIs. Figures E1(a) and E2(a) show the two dimensional histograms in a grayscale corresponding to the normalized logarithmic probability density $\log_{10}(P \cdot 2\pi\sqrt{|\Sigma_E|e})$, i.e., the logarithm of the probability density (P) normalized by the 1σ probability density ($e^{-1/2}/(2\pi\sqrt{|\Sigma_E|})$) where $|\Sigma_E|$ is the determinant of the covariance matrix Σ_E calculated from the estimated probability distribution. Thus, the correspondence between the zero crossing regions and a 1σ equiprobability curve is a good measure of the accuracy of an analytical result. Figures E1(b) and E2(b) and Figs. E1(c) and E2(c) show the cross sections of the PDFs at the deterministic equilibrium points with fixed CI and fixed LacI, respectively.

Both Figs. E1 and E2 show that the analytical results are in good agreement with the simulations. Note that the analytical representation of the 2 variable model (Eq. (21)) and applying the LNA directly to the full 12 variable model (result not shown) yield almost the same results.

E.2 Mutually repressive network

The comparisons between the LNA and the stochastic simulation are shown for two parameters: [IPTG]=10μM in Fig. E3 and [IPTG]=20μM in Fig. E4. The initial values of all the sample paths are set at the deterministic lower-right equilibrium point for each parameter; the number of the sample paths is 16000 and the length of each path is 40000s. Figures E3(a) and E4(a), Figs. E3(b) and E4(b), and Figs. E3(c) and E4(c) show the two dimensional histograms, the CI fixed cross sections, and the LacI fixed cross sections, similarly to those in the autoregulatory network. The cross sections are shown at the lower-right equilibrium points.

Figures E3(a)(b) and E4(a)(b) show the good agreement of the analytical results to the simulations. The true PDFs are far from Gaussian when the copy numbers are extremely small (see Figs. E3(c) and E4(c)). However, the analytical results approximate the true PDFs fairly well even in these cases. Similarly to the autoregulatory network, the

analytical representation (Eq. (21)) and applying the LNA directly to the full 12 variable model (result not shown) yield almost the same results.

Figure Legends

Figure 1: (a) A reaction model of a single-gene autoregulatory network. This model consists of two molecular species, the monomer and dimer forms of the expressed protein, and four reactions, namely, protein synthesis, dimerization, dissociation, and degradation. The dimers formed in solution repress the transcription of the gene.

(b) Noise Reduction by autoregulation. The noise ellipsoids show the shapes of the Gaussian distributions in the normalized coordinate system. The negative feedback strength ρ is increased from $\rho = 0$ (no repression) to $\rho = 367$ (strong repression). The direction of the *protein birth and death noise* (chained line) and the *monomer-dimer fluctuation noise* (dotted line) are shown.

(c) The parameter space plot with the transcription initiation rate α and the negative feedback strength ρ as x- and y-axes, respectively. Equi-noise (η_{max}) curves (solid curves) are shown. Each short arrow represents the maximum noise direction ($\boldsymbol{v}_{max}$) at the corresponding parameter value.

(d) Control of the direction of noise by changing the dimer dissociation constant K_d. The crosses show the equilibrium points. The noise ellipsoids show the 1σ equiprobability curves of the probability distributions around the equilibrium points. The direction of the *protein birth and death noise* (chained line) and the *monomer-dimer fluctuation noise* (dotted line) are shown.

Figure 2: (a) A reaction model of a two-gene autoregulatory network. This model consists of two molecular species, protein species $\mathcal{A}$ and $\mathcal{B}$, and four reactions, namely, syntheses and degradations of $\mathcal{A}$ and $\mathcal{B}$. The protein $\mathcal{A}$ represses the transcription of the *gene b* and the protein $\mathcal{B}$ activates the transcription of the *gene a*.

(b) Control of the direction of noise by genetic regulation. Noise ellipsoids are shown for different values of the positive regulatory strength ρ_α (broken lines) or the negative regulatory strength ρ_β (solid lines). The chained lines and the dotted lines show the directions denoted by the two vectors $(1, -\rho_\beta)^{\mathrm{T}}$ and $(\rho_\alpha, 1)^{\mathrm{T}}$, respectively.

(c) The parameter space plot with the positive regulatory strength ρ_α and the negative regulatory strength ρ_β as x- and y-axes, respectively. Equi-noise (η_{max}) curves

(solid curves) are shown. Each short arrow represents the maximum noise direction ($\boldsymbol{v}_{max}$) at the corresponding parameter value.

Figure 3: (a) A biologically plausible two-gene autoregulatory network. The *lacI*-Ptrc-2 and the *cI*-$\mathrm{P_{RM}}$ gene-promoter yield negative and positive regulations, respectively. IPTG is the inducer that inactivates the repression of Ptrc-2 promoter by *lacI*.

(b) Control of the shape of the probability distribution by IPTG induction. The IPTG concentration is increased from 16μM to 400μM. The nullclines of Eqs. (17) and (18) with regulatory functions denoted by Eqs. (22) and (23) are shown. The noise ellipsoids are shown at each equilibrium point for each IPTG concentration. The results of stochastic simulations are also shown (see noise ellipsoids in broken lines).

(c) Control of the direction of noise by IPTG induction. The noise ellipsoids in the normalized coordinate system are shown from [IPTG]=16μM to [IPTG]=400μM.

Figure 4: (a) A two-gene mutually repressive switch (Gardner *et al.*, 2000). The *lacI*-Ptrc-2 and the *cI*-$\mathrm{P_L}$ gene-promoter pairs yield mutual repression. IPTG is the inducer that inactivates the repression of Ptrc-2 promoter by *lacI*.

(b) Noise in IPTG induced genetic switching. The IPTG concentration is increased from a bistable state ([IPTG]=0 μM) to just before ([IPTG]=20μM) the deterministic bifurcation ([IPTG]=20.184 μM). The nullclines of Eqs. (17) and (18) with regulatory functions denoted by Eqs. (24) and (25) are shown. The noise ellipsoids are shown at each stable equilibrium point for each IPTG concentration. Crosses and circles represent stable equilibrium points and saddle points, respectively.

Figure B1: The overall picture of the decoupling of a stoichiometric matrix, the diagonalization of a diffusion matrix, and the decomposition of noise.

Figure B2: The bipartite graph of the original (left, see Eq. (B.1)) and decoupled (right, see Eq. (B.2)) stoichiometric matrices. A bipartite graph (U,V,E) of a stoichiometric matrix A is defined as follows (Temkin *et al.*, 1996): $\mathrm{U} = \{\mathrm{u}_j\}_{j=1,\ldots,M}$ is the set of vertices corresponding to reaction channels. $\mathrm{V} = \{\mathrm{v}_i\}_{i=1,\ldots,N}$ is the set of vertices corresponding to molecular species. $\mathrm{E} = \{\mathrm{e}_{ij}\}$ is the set of edges. e_{ij} denotes the edge between u_j and v_i. Here, e_{ij} exists if and only if $a_{ij} \neq 0$. Note that

the stoichiometric matrix that a bipartite graph represents is not unique in this definition, which is sufficient for the current purpose.

Figure E1: Stochastic simulation of the two-gene autoregulatory network in section 3.3 with [IPTG]=16μM. (a) The two dimensional histogram of the simulation result and the LNA (the noise ellipsoid in broken line). The histogram is shown in a grayscale, corresponding to the logarithmic probability density normalized by the 1σ probability density $\log_{10}(P \cdot 2\pi\sqrt{|\Sigma_E|e})$.

(b) The cross section of the probability density function with CI fixed at the deterministic equilibrium point. (c) The cross section of the probability density function with LacI fixed at the deterministic equilibrium point.

Figure E2: Stochastic simulation of the two-gene autoregulatory network in section 3.3 with [IPTG]=252μM. (a)(b)(c) are similar to those in Fig. E1.

Figure E3: Stochastic simulation of the two-gene mutually repressive network in section 3.4 with [IPTG]=10μM. The initial values for the sample paths are set at the lower-right equilibrium point. (a)(b)(c) are similar to those in Fig. E1.

Figure E4: Stochastic simulation of the two-gene mutually repressive network in section 3.4 with [IPTG]=20μM. The initial values for the sample paths are set at the lower-right equilibrium point. (a)(b)(c) are similar to those in Fig. E1.

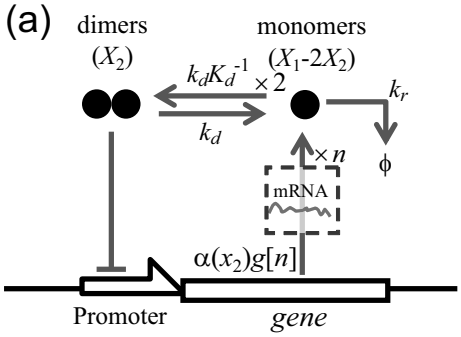

Figure 1(a)
Tomioka *et al.*

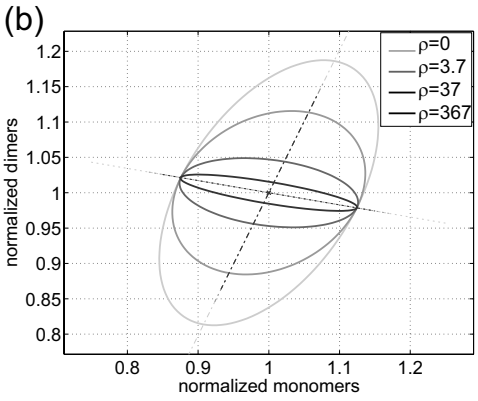

Figure 1(b)
Tomioka *et al.*

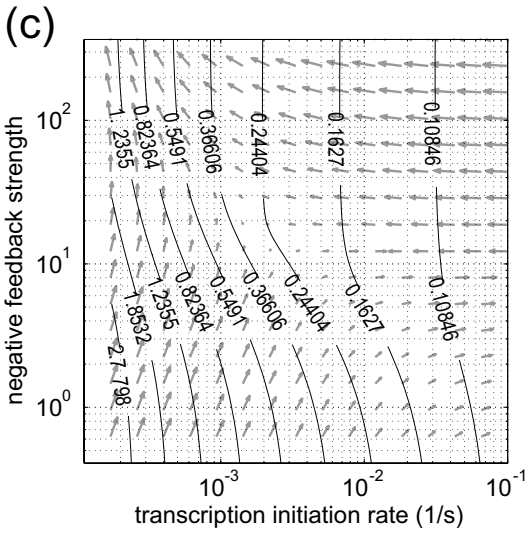

Figure 1(c)
Tomioka *et al.*

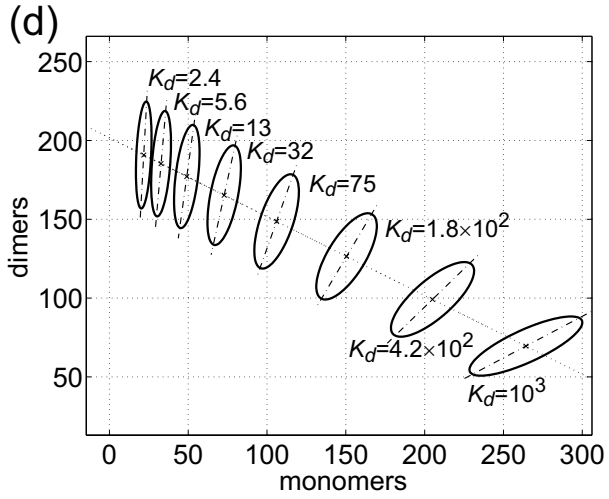

Figure 1(d)
Tomioka *et al.*

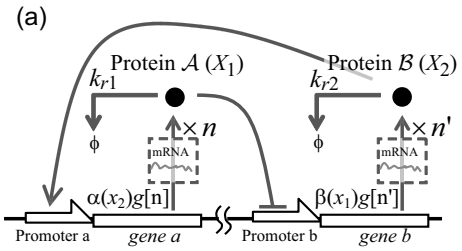

Figure 2(a)
Tomioka *et al.*

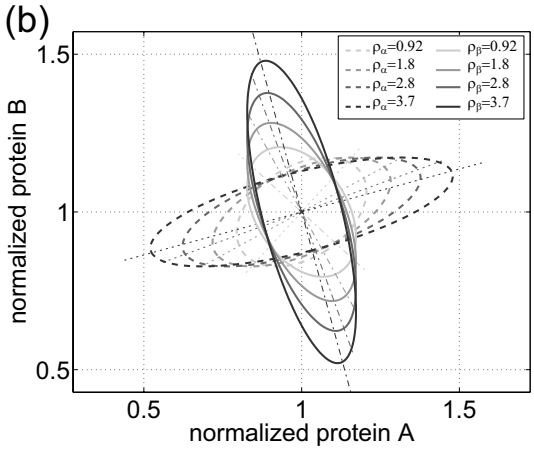

Figure 2(b)
Tomioka *et al.*

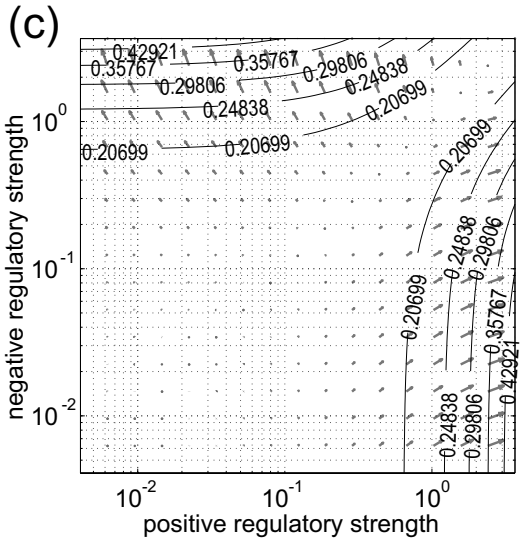

Figure 2(c)
Tomioka *et al.*

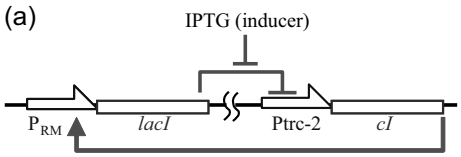

Figure 3(a)
Tomioka *et al.*

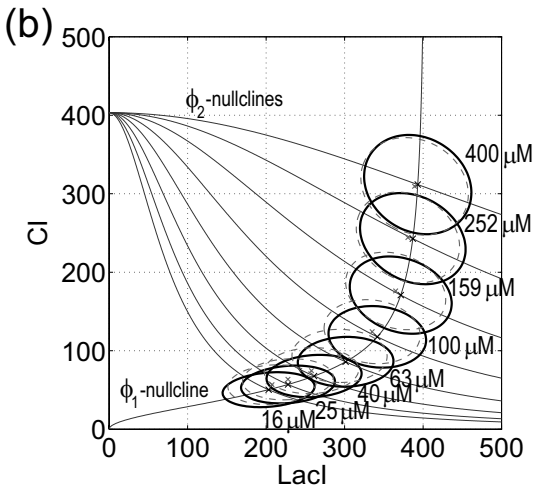

Figure 3(b)
Tomioka *et al.*

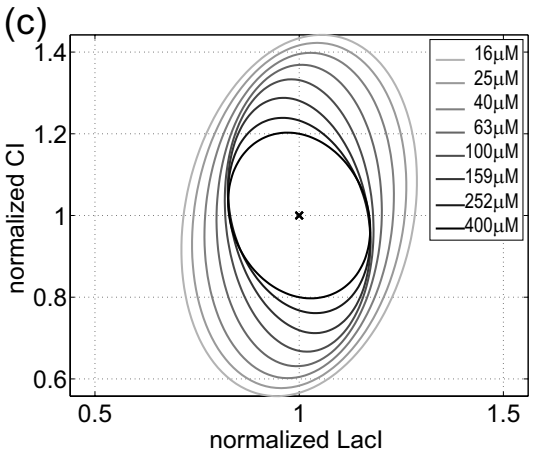

Figure 3(c)
Tomioka *et al.*

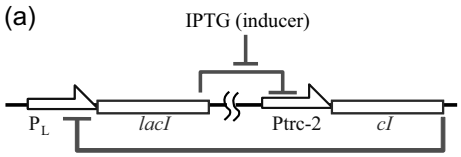

Figure 4(a)
Tomioka *et al.*

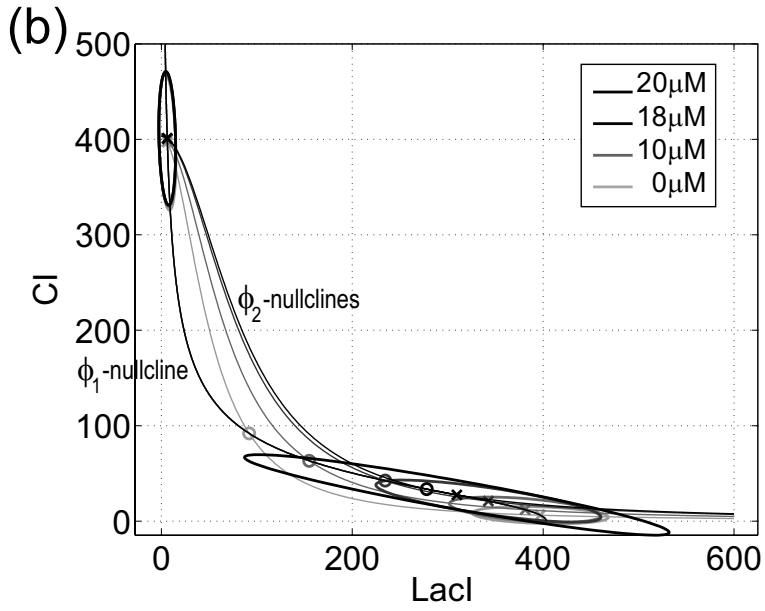

Figure 4(b)
Tomioka *et al.*

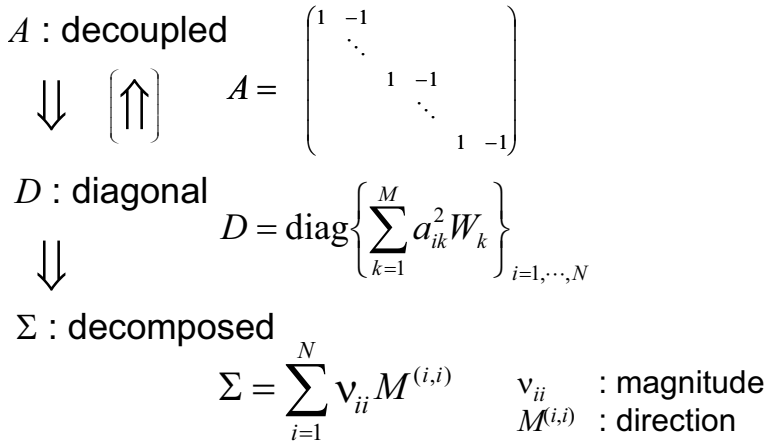

Figure B1
Tomioka *et al.*

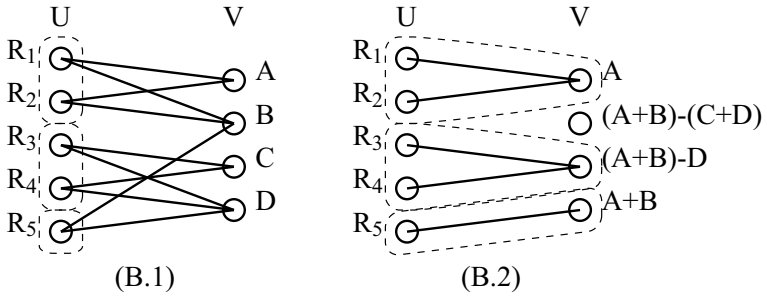

Figure B2
Tomioka *et al.*

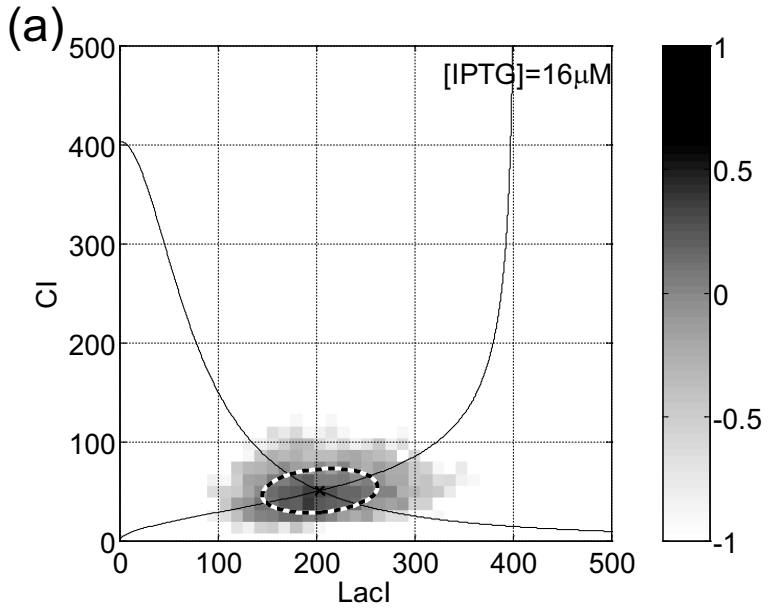

Figure E1(a)
Tomioka *et al.*

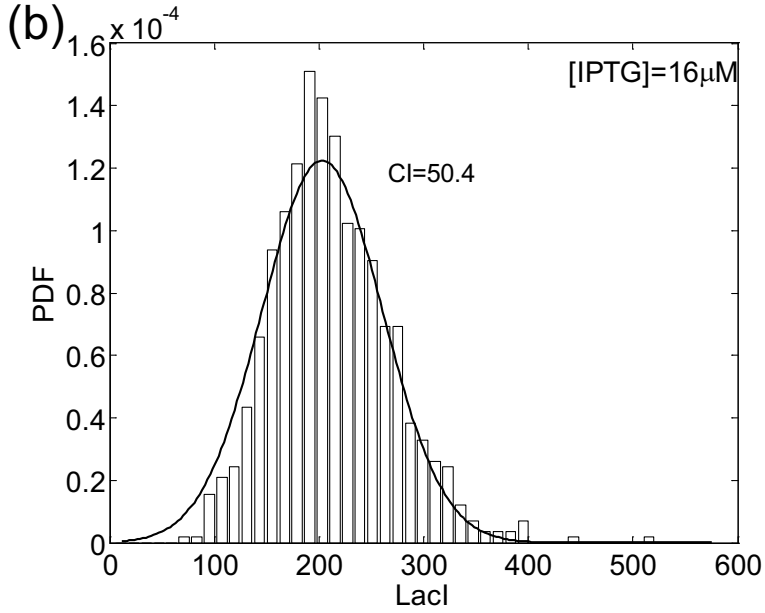

Figure E1(b)
Tomioka *et al.*

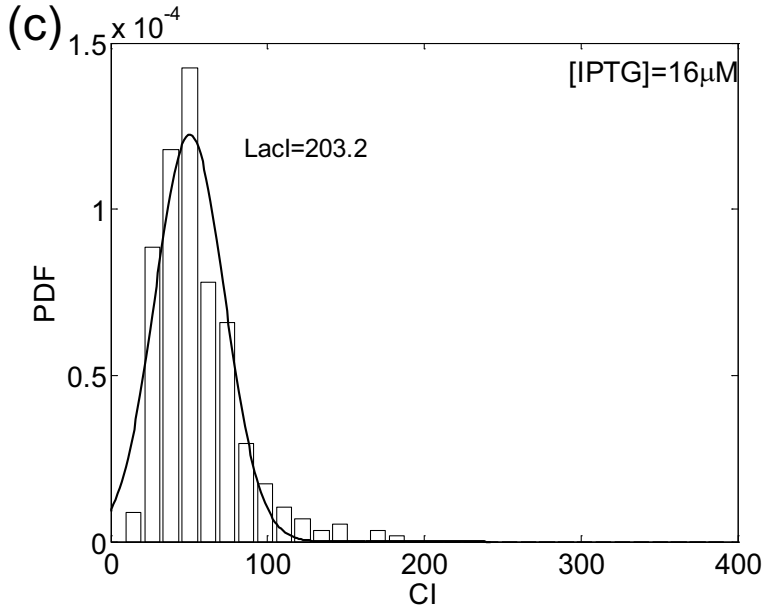

Figure E1(c)
Tomioka *et al.*

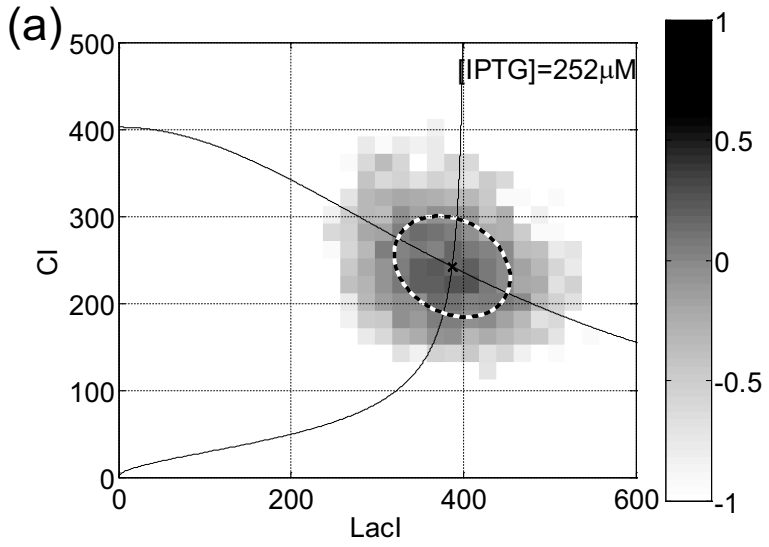

Figure E2(a)
Tomioka *et al.*

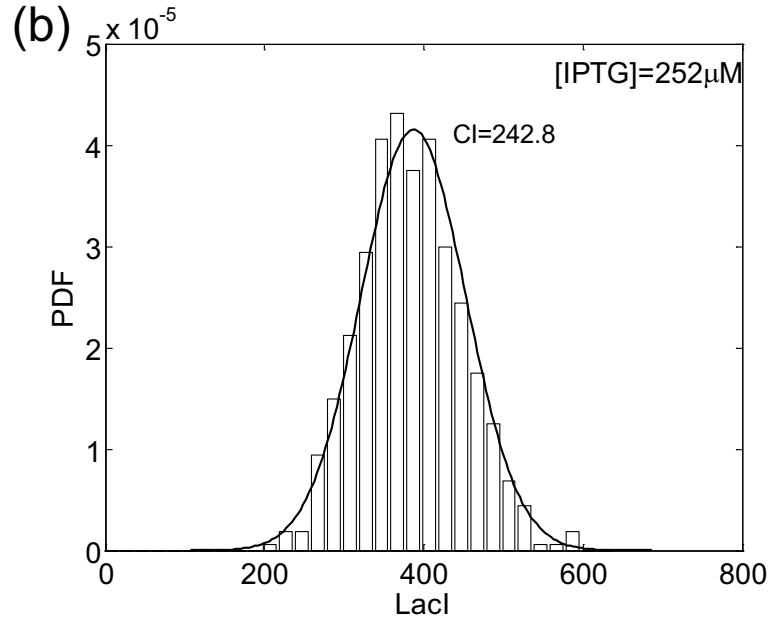

Figure E2(b)
Tomioka *et al.*

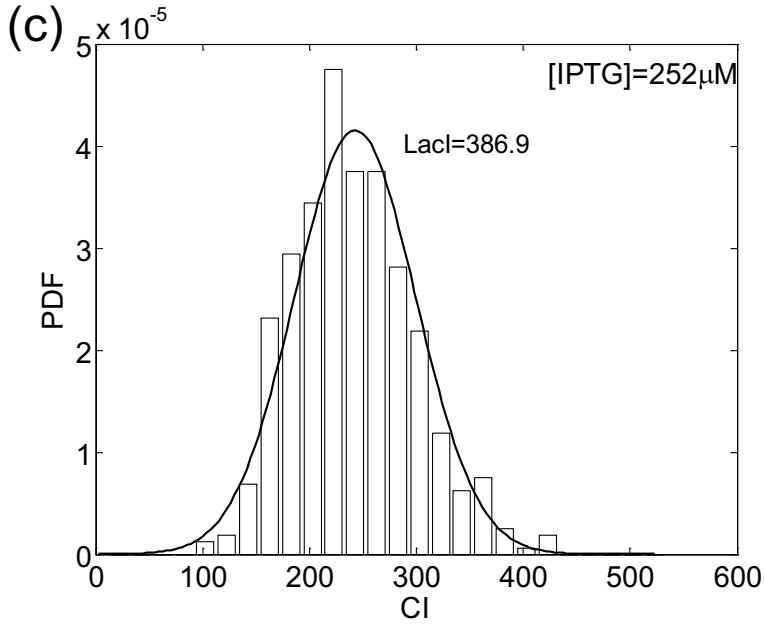

Figure E2(c)
Tomioka *et al.*

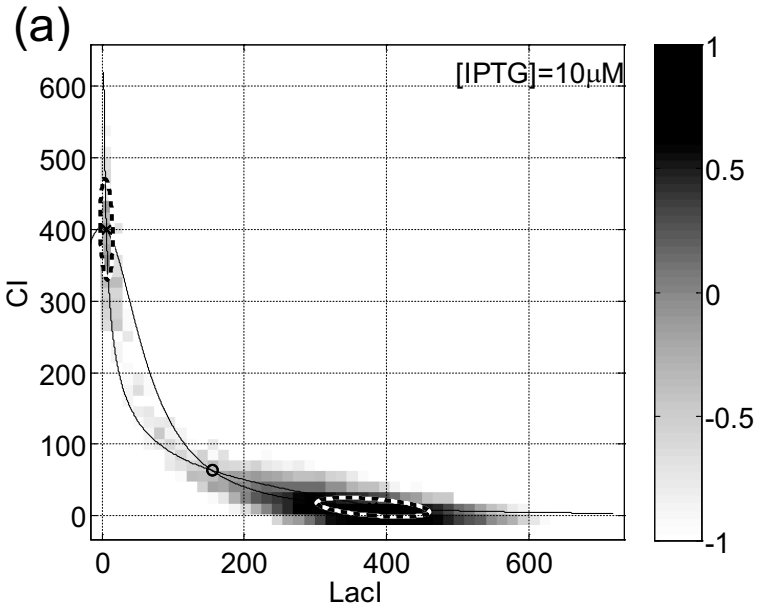

Figure E3(a)
Tomioka *et al.*

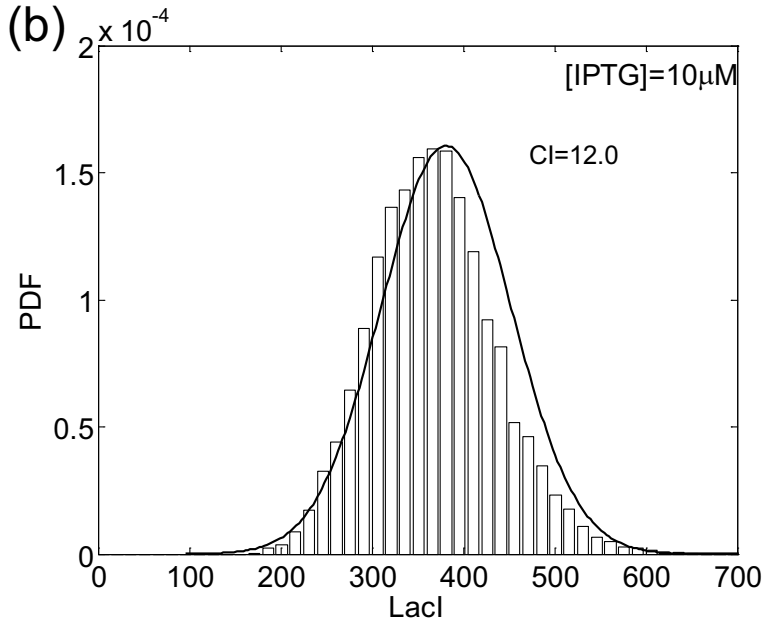

Figure E3(b)
Tomioka *et al.*

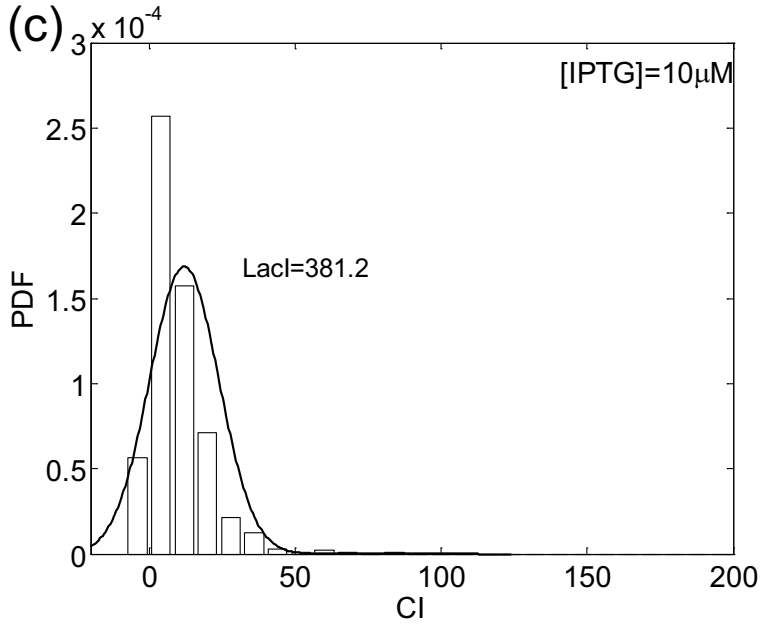

Figure E3(c)
Tomioka *et al.*

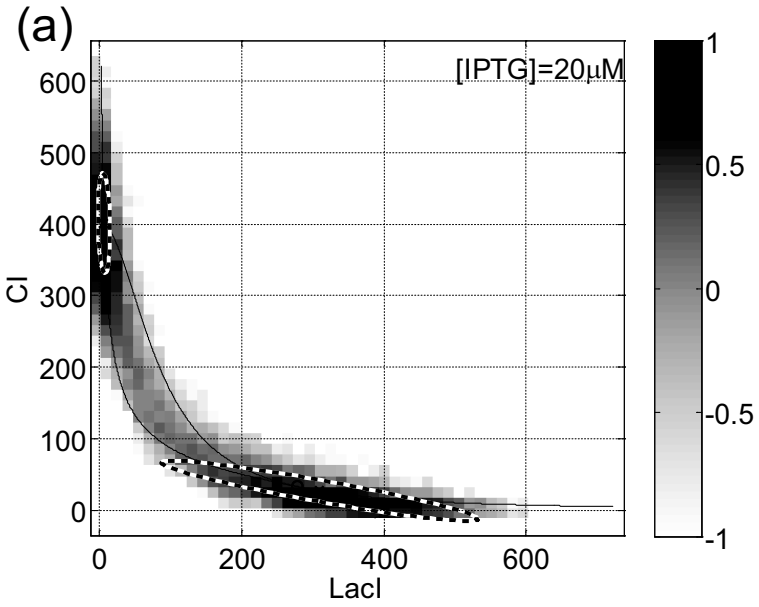

Figure E4(a)
Tomioka *et al.*

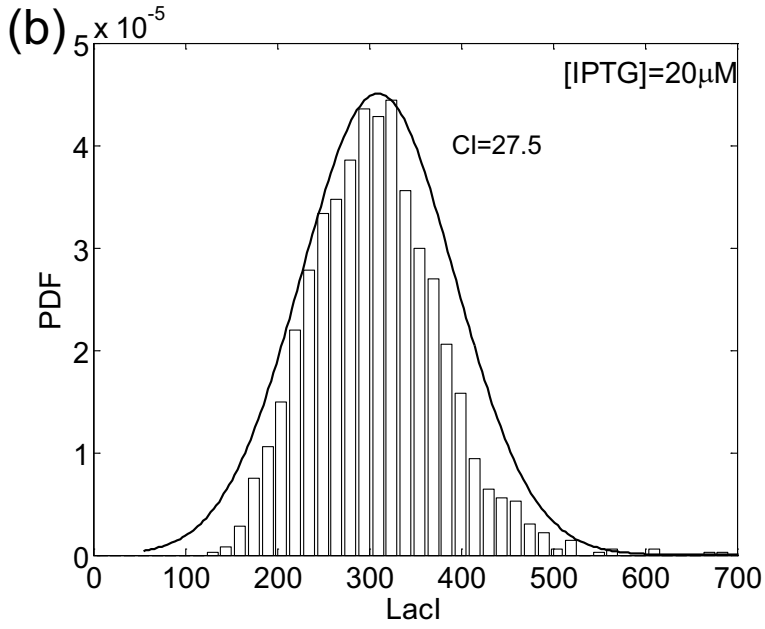

Figure E4(b)
Tomioka *et al.*

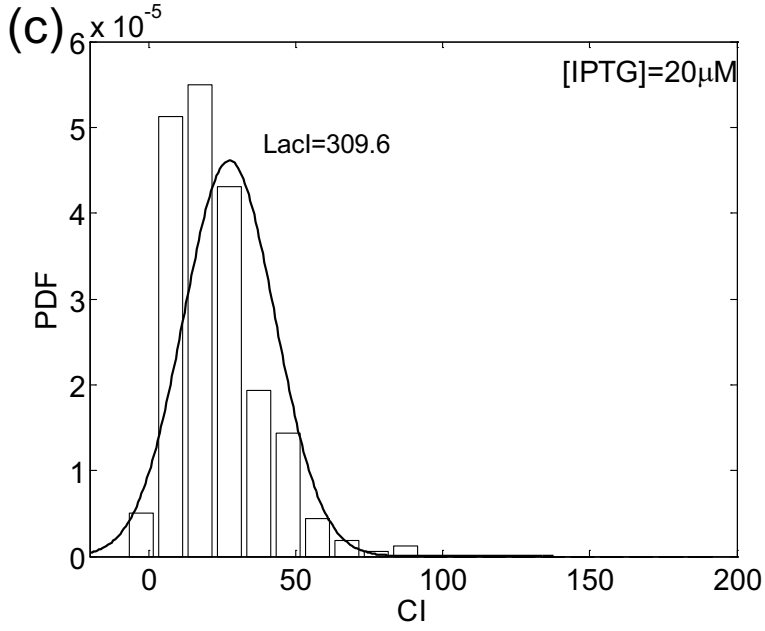

Figure E4(c)
Tomioka *et al.*

Table D1: Parameter values used for the single-gene autoregulatory network.

Parameters	Values
cell volume	$\Omega = 10^9$ $\left(= 1.66 \times 10^{-15}(\text{liters}) \cdot 6.02 \times 10^{23}\right)$
transcription initiation rate	$\alpha = 0.011$ (s^{-1})
negative feedback strength	$\rho = 0$
average protein synthesis per mRNA	$B = 11$ (proteins/mRNA)
dimer dissociation constant	$K_d = 20$ (nM)
dimer dissociation rate constant	$k_d = 1$ (s^{-1})
protein degradation rate constant	$k_r = 0.0003$ (s^{-1})

Table D2: Parameter values for the two-gene autoregulatory network.

Parameters	Values
cell volume	$\Omega = 10^9$ $\left(= 1.66 \times 10^{-15}(\text{liters}) \cdot 6.02 \times 10^{23}\right)$
transcription initiation rate	$\alpha = \beta = 0.011$ (s^{-1})
positive regulatory strength	$\rho_\alpha = 0$
negative regulatory strength	$\rho_\beta = 0$
average protein synthesis per mRNA	$B_1 = B_2 = 11$ (proteins/mRNA)
protein degradation rate constant	$k_{r1} = k_{r2} = 0.0003$ (s^{-1})

Table D3: Parameter values for the biologically plausible two-gene autoregulatory network and the two-gene mutually repressive network.

Parameters	Values
cell volume	$\Omega = 10^9 \ \left(= 1.66 \times 10^{-15}(\text{liters}) \cdot 6.02 \times 10^{23}\right)$
maximum transcription initiation rate	$\alpha_0 = \beta_0 = 0.011 \ (\text{s}^{-1})$
DNA-regulatory protein binding constant	$K_\alpha = K_\beta = 50 \ (\text{nM})$
DNA-regulatory protein binding Hill coefficient	$h_\alpha = h_\beta = 2$
average protein synthesis per mRNA	$B_1 = B_2 = 11 \ (\text{proteins/mRNA})$
protein degradation rate constant	$k_{r1} = k_{r2} = 0.0003 \ (\text{s}^{-1})$
IPTG-LacI binding constant	$K_I = 29.618 \ (\mu\text{M})$
IPTG-LacI binding Hill coefficient	$h_I = 1$

Table E1: Parameter values for the full models of biologically plausible two-gene autoregulatory network and two-gene mutually repressive network.

Parameters	Values
cell volume	1.66×10^{-15}(liters)
k_1	$1\,(\mathrm{nM}^{-1}\mathrm{s}^{-1})$
k_2	$2500\,(\mathrm{s}^{-1})$
k_3	$1\,(\mathrm{nM}^{-1}\mathrm{s}^{-1})$
k_4	$1\,(\mathrm{s}^{-1})$
k_5	$0.011\,(\mathrm{s}^{-1})$
k_6	$1.1\,(\mathrm{s}^{-1})$
k_7	$0.1\,(\mathrm{s}^{-1})$
k_8	$0.1\,(\mu\mathrm{M}^{-1}\mathrm{s}^{-1})$
k_9	$2.962\,(\mathrm{s}^{-1})$
k_{10}	$0.0003\,(\mathrm{s}^{-1})$
k_{11}	$0.0003\,(\mathrm{s}^{-1})$
k_{12}	$1\,(\mathrm{nM}^{-1}\mathrm{s}^{-1})$
k_{13}	$2500\,(\mathrm{s}^{-1})$
k_{14}	$1\,(\mathrm{nM}^{-1}\mathrm{s}^{-1})$
k_{15}	$1\,(\mathrm{s}^{-1})$
k_{16}	$0.011\,(\mathrm{s}^{-1})$
k_{17}	$1.1\,(\mathrm{s}^{-1})$
k_{18}	$0.1\,(\mathrm{s}^{-1})$
k_{19}	$0.0003\,(\mathrm{s}^{-1})$